2021

FXR AGONISTS INDUCE DISTINCT H-12 STRUCTURAL STATES

Vikash Kumar

FXR AGONISTS INDUCE DISTINCT H-12 STRUCTURAL STATES

By

VIKASH KUMAR

Thesis

presented in partial fulfillment of the requirements
for the degree of

Master of Science
in Biochemistry and Biophysics

The University of Montana
Missoula, MT

June 2021

Approved by:

Scott Whittenburg, Dean of The Graduate School
Graduate School

Bruce Bowler, Chair
Chemistry and Biochemistry

Travis Hughes, Advisor
Biomedical and Pharmaceutical Sciences

Steve Sprang
Division of Biological Sciences

J.B. Alexander (Sandy) Ross
Chemistry and Biochemistry

Jesse Hay
Division of Biological Sciences

Kumar, Vikash, MS, Spring 2021 Biochemistry and Biophysics

FXR AGONISTS INDUCE DISTINCT H-12 STRUCTURAL STATES

Chairperson: Bruce Bowler

Thesis Advisor: Travis Hughes

The nuclear receptor ligand-binding domain (LBD) is a highly dynamic entity. The FXR LBD shows multiple low-energy conformational states of the activation function-2 (AF-2) coregulator binding surface upon ligand binding, indicating the complexity of FXR activation. However, it is unknown how ligand binding leads to different conformational states within the AF-2 region centered on helix 12 (H-12) of the LBD. Here we observe the conformation of the coregulator binding surface (H-12 specifically) of FXR upon ligand binding in solution using fluorine-19 (19F) nuclear magnetic resonance (NMR) and simulations of this surface using molecular dynamics. Fluorescence anisotropy of fluorescein-labeled coregulator peptides reveals a correlation between structural conformations of the coregulator binding surface and the function of FXR. While the coregulator surface of apo FXR and partial-agonist bound FXR exchanges between multiple low energy conformations, full-agonist bound FXR is restricted to few conformations, which favor coactivator binding. Furthermore, we find that two ligands that induce similar affinities for a coactivator peptide have distinct coregulator binding surface structures.

TABLE OF CONTENTS

LIST OF TABLES

Table Page No.

LIST OF FIGURES

Figure Page No.

CHAPTER I

INTRODUCTION

Farnesoid X receptor (FXR) is a ligand-activated transcription factor,[1] found mainly in the liver and kidney[2]. FXR maintains the homeostasis of bile acids, vital for metabolic regulation and liver protection by regulating bile acids[3]. Like other nuclear receptors (NR) superfamily members, FXR recruits coregulators upon ligand binding, thereby changing the expression level of genes involved in bile acid, glucose, and lipid metabolism. Because it regulates bile acids in the liver, FXR is a potential drug target for treating several liver-related disorders, including nonalcoholic steatohepatitis (NASH) and primary biliary cholangitis (PBC), and diabetes[4,5].

Partial FXR activation is a promising strategy to target liver disorders and to reduce mechanism-based side effects. Partial Nuclear Receptor agonists have lower gene activation efficacy than full agonists**,** and promising results have been seen for partial FXR agonists in pre-clinical and phase 1 clinical data[6].

The ligand-binding mechanism to the ligand-binding domain (LBD) of an NR and the structural changes that occur upon binding that lead to gene expression changes differ among NRs[7]. Therefore, the structural changes that lead to FXR activation are unclear.

NR structure is highly conserved, consisting of a set of standard functional domains. A highly variable N-terminal ligand-independent activation domain followed by a highly

conserved DNA-binding domain (DBD) and a ligand-binding domain (LBD) that consists of twelve alpha-helices (H-1 to H-12). A flexible hinge region separates LBD from DBD. There are two coregulator binding activation function (AF) sites; AF-1 is located on N-terminus while AF-2 is on the C-terminus (H-12 of LBD). For several nuclear receptors, the AF-2 site is crucial for NR activation by small-molecule ligands. Ligand binding changes the conformation of the AF-2 helix, providing a surface for coactivator binding[8].

Previous studies have suggested a mousetrap model for NR activation in which H-12 is positioned away from the core LBD in the apo state, which switches to a more compact structure with H-12 contacting the core LBD upon ligand binding[9]. Later studies have revised this mouse trap model of activation. They suggest that H-12 is dynamic and possibly non-helical in the apostate, and H-12 is only formed and stabilized upon agonist binding. This model suggests that more than a single active conformation of NR-LBDs exists[10]. Studies have already shown differential effects of FXR agonists on FXR regulated gene expression, implying that FXR activation is more complex than the mechanism described by the mousetrap model[11]. Different FXR ligands lead to different coactivator recruitment profiles[12,13]. This phenomenon has also been reported for other NRs, including PPARγ[14].

To better understand FXR activation and observe different conformational states of H-12 upon binding of FXR ligands, we have used ligands that have been previously characterized in cells as agonists and antagonists for structural investigation. We employ 19F-NMR and molecular dynamics (MD) simulation to determine how ligand binding

changes the conformation of the FXR LBD. Our study indicates that a full agonist induces different conformational states than two partial agonists, which induce different FXR states from each other. However, one of them induces similar states as that of apo. Thus, this work enhances our understanding of FXR activation and partial FXR agonism.

1. Nuclear Receptor (NR)

Hydrophobic messenger molecules such as steroid hormones, retinoids, and free fatty acids control many aspects of developmental, reproductive, and metabolic processes in eukaryotes[15]. These molecules require carrier proteins (globulins) for their distribution; they can enter the plasma membrane and are captured by intracellular receptors. These "nuclear receptors" (NRs) are DNA-binding proteins that act as transcription factors[16]. Thus, the NR are ligand-activated transcriptional factors that principally act by binding DNA and controlling transcription.

1.1 NR structure

NR superfamily members share a standard modular domain structure, consisting of five domains: A-E (**Fig. 1**). Each of these domains plays a crucial role in NR biology.

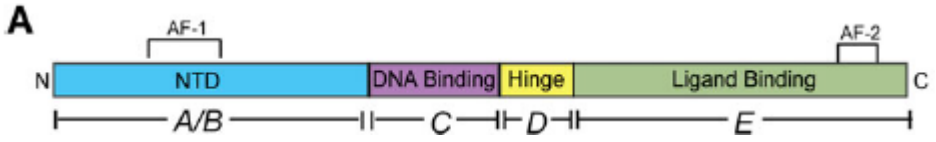

Fig. 1: Domain structure of NRs. [Figure adapted from *Weikum et al., 2018*][17]

A/B: N-terminal domain (NTD): The NTD is a highly disordered domain with little sequence conservation and significant size differences among NRs. The NTD contains the activation function-1 (AF-1) region, which interacts with coregulators in a cell in a promoter-specific manner and, in general, is disordered. Variability in this region produces multiple isoforms via alternative splicing and is a target for many post-translational modifications[18].

C: DNA binding domain (DBD): The DBD is the most conserved region among all members of the NR superfamily. DBD consists of two subdomains. Each consists of four cysteine residues that coordinate a zinc ion to form a canonical DNA-binding zinc finger motif[17,19] (**Fig. 2**).

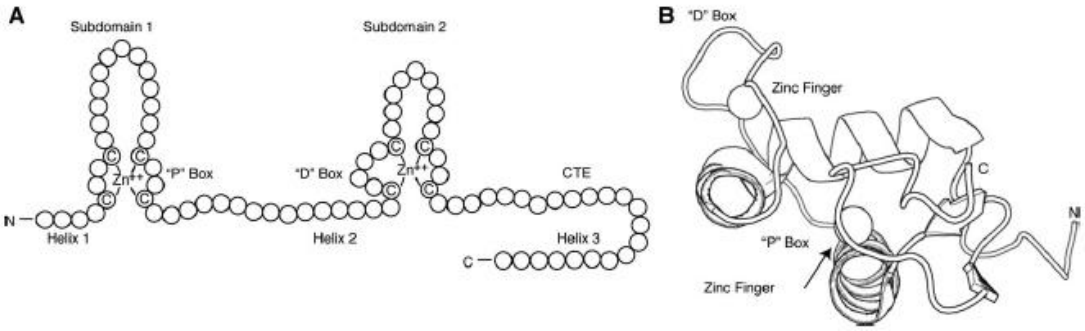

Fig. 2: NR DNA binding domain (a) NR DBD indicating significant motifs (b) folded DBD indicating essential regions. [Figure adapted from *Weikum et al., 2018*][17]

D: Hinge region: A short and flexible region that separates the DBD and LBD. The hinge region has low sequence and size conservation among NRs.

E: Ligand Binding domain (LBD): The LBD is comprised of approximately 12 alpha-helices, which form three antiparallel helical layers described as an alpha-helical sandwich. The LBD binds ligands in the ligand-binding pocket (LBP) and contains the primary surfaces involved in homodimerization or heterodimerization with other nuclear receptors. The LBP is primarily a hydrophobic internal pocket surrounded by helices (**Fig. 3**). The LBP is variable among NRs compared to other parts of LBD, which allows it to recognize a diverse group of ligands.

The LBD also contains the AF-2 region consisting of helices 3, 4, and 12. The binding of ligand to LBP changes the conformation of the AF-2 region to facilitate interaction with different coregulator proteins (**Fig. 3**).

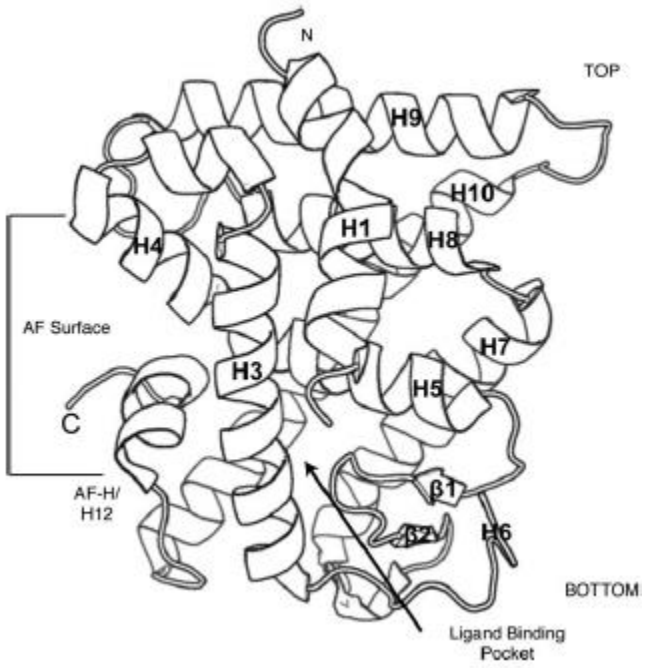

Fig. 3: Cartoon representation of structurally conserved NR LBD and its various regions. [Figure adapted from *Weikum et al., 2018*][17]

1.2 NR structure-function relation

NR function is determined by two globular structural domains: a moderately conserved C-terminal LBD and a highly conserved and centrally located DBD. The LBD serves essential functions as it contains an LBP specific for its cognate hormone or ligand and an AF-2 region important for recruiting various coregulator proteins.

The DBD docks the NR to the hexanucleotide response elements located within nuclear receptor-regulated promoters, leading to various transcriptional outputs. After DNA binding NR recruits coregulators which then interact with chromatin-remodeling proteins and control the general transcriptional machinery[15,20].

1.3 NR classification

NRs are classified into four subtypes [17]

Type 1 NRs: These steroid receptors are activated by cholesterol-derived steroidal hormones. Type I NRs are found in the cytoplasm bound to chaperone proteins, but upon binding of ligand undergo nuclear translocation where they generally bind as homodimers to DNA response elements (**Fig. 4a**). An example of a type 1 NR is the estrogen receptor (ER).

Type 2 NRs: These NRs are generally retained in the nucleus and swap corepressor to coactivator upon ligand binding. They generally form heterodimers with RXR (retinoid X receptor, a common heterodimeric partner of many NRs) when bound to DNA response elements (**Fig. 4b**). An example of a type 2 NR is the retinoic acid receptor (RAR).

Type 3 NRs: These NRs have a mechanism of action similar to type 2 NRs but form homodimers when bound to DNA response elements (**Fig. 4c**). An example of a type 3 NR is the Vitamin D3 receptor (VDR)

Type 4 NRs: These NRs have a mechanism of action similar to type 2 NRs but bind to DNA response elements as a monomer (**Fig. 4d**). An example of a type 4 NR is Liver receptor homolog 1 (LRH-1).

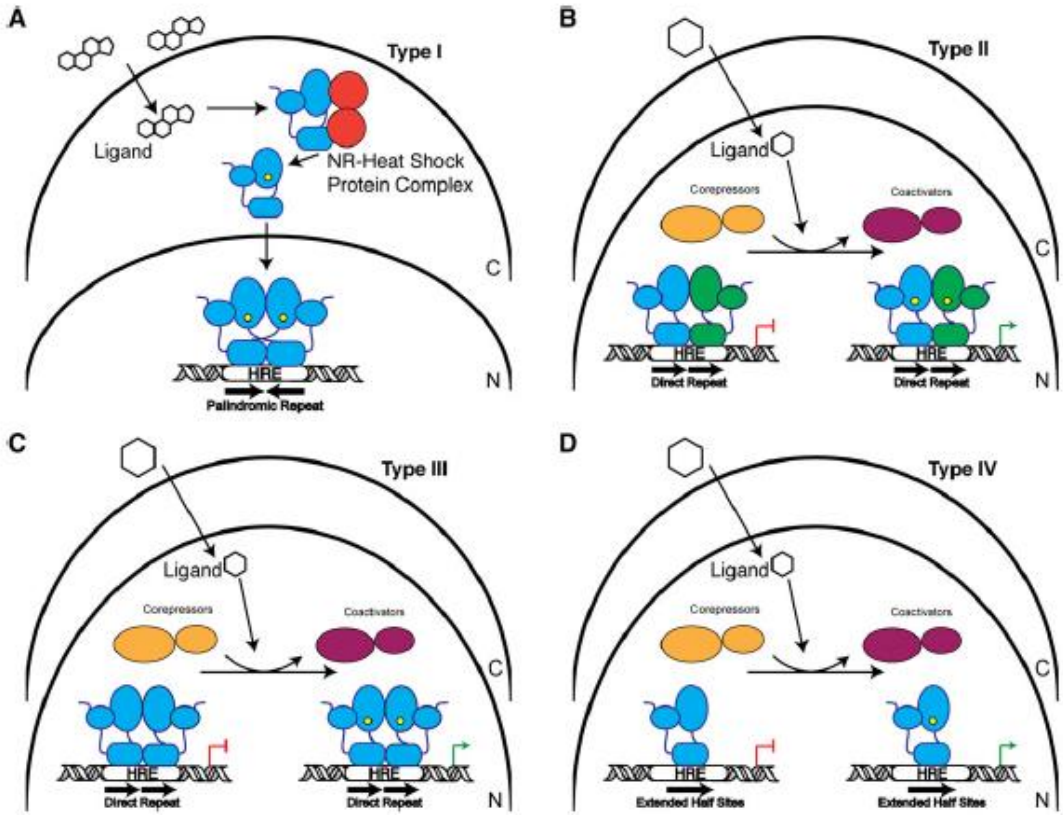

Fig. 4: NRs signaling mechanism. (a) type 1 (b) type 2 (c) type 3 (d) type 4. The color scheme is as follows, NR (blue), chaperone protein (red), RXR (green), coactivator (purple), and corepressor (orange). [Figure adapted from *Weikum et al., 2018*] [17]

1.4 NRs as a drug target

NRs regulate many physiological processes such as metabolism, inflammation, reproduction, and development. NR activities are tightly controlled as they are responsible for regulating many genes[21,22]. Therefore, any disorder in NR activity can lead to numerous diseases such as diabetes, cancer, and chronic inflammation[23,24]. Structural and genomic studies of NRs have helped develop synthetic ligands targeting these receptors. However, since NRs regulate many genes and many ligands are not specific to a given NR, ligand binding often leads to both desired and undesired effects. A better understanding of the NR regulation mechanism could help identify ligands that affect only a subset of all NR-regulated genes instead of all the genes under the control of a given NR.

2. Farnesoid X Receptor (FXR)

Farnesoid X receptor (FXR) is a ligand-activated transcription factor of the nuclear receptor type 2, superfamily[1]. Bile acids are physiological ligands for FXR; hence FXR is also known as the bile acid receptor.

Bile acids are essential for the solubilization and transport of dietary lipids and a significant product of the enzymatic conversion of cholesterol. Bile acid bound FXR represses transcription of the gene encoding cholesterol 7α-hydroxylase, the rate-limiting enzyme in bile acid synthesis, and activates the gene encoding intestinal bile acid-binding protein, a candidate BA transporter, indicating a mechanism by which BA transcriptionally regulates its biosynthesis and enterohepatic transport[25].

FXR plays a crucial role in bile acid homeostasis by regulating genes involved in bile acid synthesis, conjugation, and enterohepatic circulation. In addition, FXR as a metabolic regulator also plays an essential role in cholesterol, lipid, and glucose metabolism.

2.1 FXR expression

There are two FXR genes (FXRα (NR1H4) and FXRβ (NR1H5)) in mammals[26]. FXRβ is a functional receptor in rodents but is a pseudogene in humans and primates[27]. The functional role of FXRβ is not well known. A single FXRα gene can encode FXRα1 or α2 and FXRα3 or α4 isoforms, but the physiological role of this diversity is not clearly understood[28]. Alternate splicing gives rise to the multiple isoforms which differ at the AF-1 domain, FXRα3 and FXRα4 possess an extended N-terminal AF-1 domain compared to FXRα1 and FXRα2 (**Fig. 5b**). These four isoforms are expressed in a tissue-dependent manner. FXRα is mainly expressed in the liver. FXRα1 and FXRα2 are moderately expressed in the ileum and adrenal gland, while FXRα3 and FXRα4 are abundantly expressed in the ileum and moderately expressed in the kidney[2]. The sequence of FXRα1 has been chosen as the canonical sequence (uniport.org/uniport/Q96R|1). The sequence of the FXR-LBD is conserved among all four isoforms.

2.2 FXR as a drug target

FXR plays an essential role in regulating systemic energy homeostasis and protecting many organs, including the liver and intestine. FXR as a metabolic regulator plays an important role in bile acid, lipid, cholesterol, and glucose metabolism and helps inter-organ communication, particularly the enterohepatic signaling pathway via bile acids. FXR also

plays various roles in the kidney, adipose tissue, pancreas, cardiovascular system, and tumorigenesis. Given its broad involvement in metabolism and many organs, the deregulation of FXR may lead to metabolic disorders and disease-causing abnormalities of specific organs. Such actions make FXR a potential drug target in treating metabolic diseases and several liver-related disorders, including nonalcoholic steatohepatitis (NASH), primary biliary cholangitis (PBC), diabetes, dyslipidemia, and obesity[30,31]. Many FXR agonists have been developed and are undergoing pre-clinical and clinical trials. For example, obeticholic Acid (OCA) is a promising candidate for treating liver and metabolic disorders, but it has some safety issues. The U.S. food and drug administration has recently approved OCA, and it is in late-stage clinical development for the treatment of NASH. Adverse effects include elevated cholesterol levels due to FXR over-activation[32-34]. This suggests that partial FXR activation may be an essential strategy to avoid mechanism-based side effects. Promising results have been reported from pre-clinical and a phase 1 clinical trial of a partial FXR agonist[6].

The effect of FXR modulation might be multifaceted according to tissue specificity and disease type, suggesting that FXR agonists must be used with care.

2.3 FXR structure

FXR shares a classic NR structure, consisting of common functional domains (**Fig. 5a**), a highly variable N-terminal ligand-independent transcriptional activation domain (AF-1), followed by a highly conserved core DNA-binding domain (DBD), a C-terminal ligand-binding domain (LBD) that consists of twelve α-helices (H-1 to H-12), a flexible hinge

region which separates LBD from DBD, and a ligand-dependent activation function domain (AF-2).

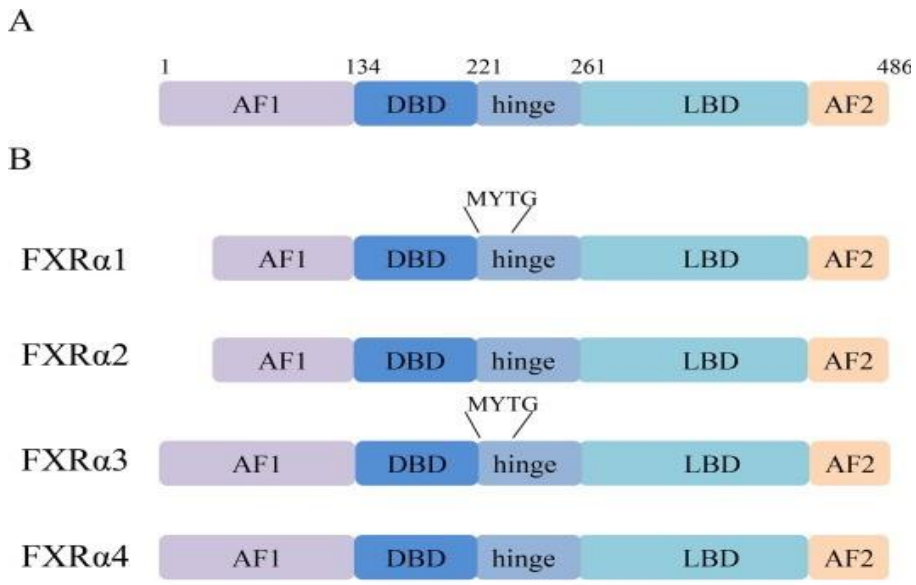

Fig. 5: Schematic diagram of FXR. (a) Structural organization of FXR (b) Schematic diagram of the four FXRα isoforms. [Figure adapted from *Jiang et al., 2021*] [29]

The AF-1 region is highly disordered and can interact with coregulator proteins. The FXR-DBD interacts with DNA in a base-specific manner which allows it to recognize a specific DNA sequence. The DBD is highly conserved and consists of two α-helices (H-1 and H-2) and two four cysteines/zinc nucleated modules[35] (**Fig. 6a**). FXRα1 and FXRα3 each have an insert of four amino acids (MYTG) in the hinge region[36] (**Fig. 5b**). The FXR-LBD binds to its cognate ligand and recruits coregulator proteins. FXR-LBD consists of 12 α-helices that fold into three parallel layers to form an alpha-helical sandwich and contains a hydrophobic ligand-binding pocket (LBP) to accommodate its ligands (**Fig. 6b**). The AF-2 region is in the LBD and includes H-12. For several nuclear receptors, the AF-2 site is

crucial for NR activation by small-molecule ligands. Ligand binding changes the conformation of the AF-2 helix, providing a surface for coactivator binding[37].

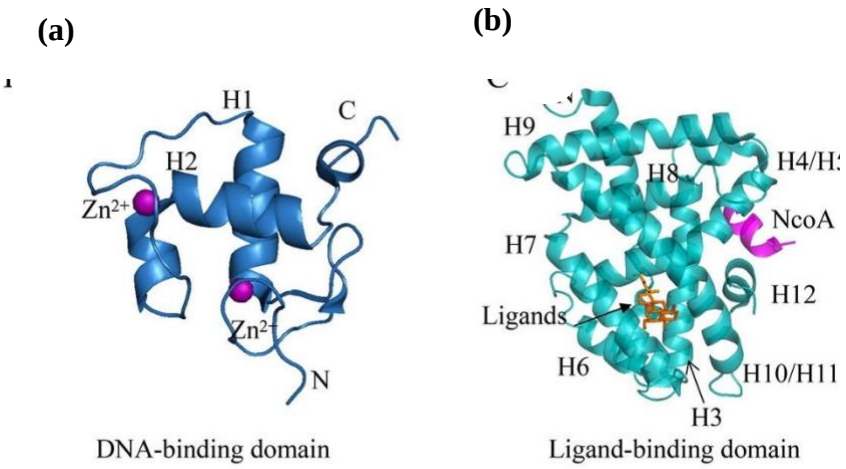

Fig. 6: (a) Model structure of FXR-DBD (PDB ID: 1R0O of EcR-DBD is used to represent FXR-DBD) (b) FXR-LBD/OCA complex (PDB ID: 1OSV), FXR-LBD is in green cyan, OCA is in orange, and NCoA peptide is in magenta. [Figure adapted from *Jiang et al., 2021*] [29]

2.4 FXR: DNA binding

FXR regulates gene expression by binding DNA as a monomer or heterodimer with RXR[38,39]. The DNA motifs recognized by FXR-DBD are called FXR response elements (FXREs) (**Fig. 7**). In the heterodimer form with RXR, the coactivator binding site (H-10/11) undergoes allosteric conformational changes, enhancing the transcriptional activity of FXR to bind FXREs[40,41]. The dimerization mechanism between FXR-DBD and RXR-DBD is still not clear. Diverse FXREs are localized in promoter, intergenic, and intron regions of many genes. The binding of FXR to FXREs leads to various biological functions such as metabolism, transport, kinase signaling, and glycolysis.

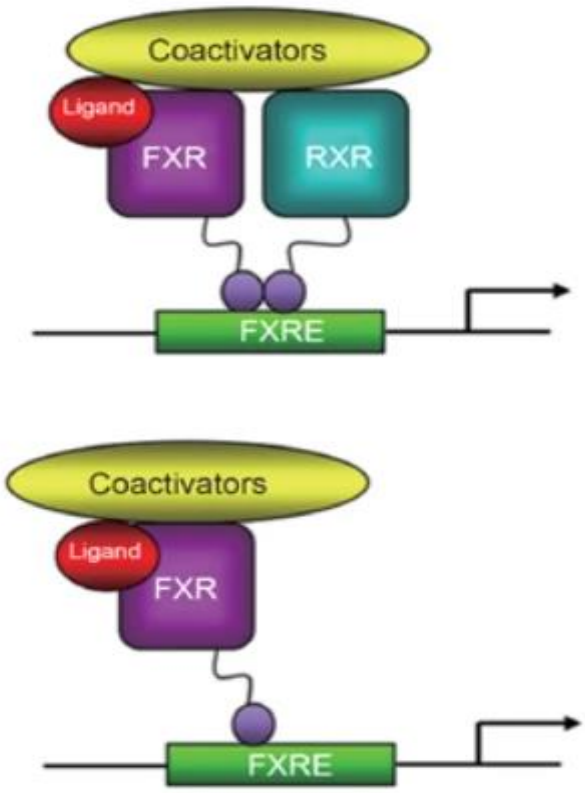

Fig. 7: FXR binds to DNA either as a heterodimer with RXR or as a monomer to regulate the expression of various genes. [Figure adapted from *Wang et al., 2018*] [40]

2.5 FXR activation: Ligand and coactivator binding

The FXR-LBD contains the ligand-binding pocket (LBP) for ligand binding. The bound ligand can adjust LBP volume [43]. Crucial polar residues (Arg, His) in the LBP form hydrogen bond interactions with ligands to position them into correct orientation, while hydrophobic residues (Ile, Phe) form hydrophobic interactions with ligands to stabilize the LBD[43,44]. Previous studies have suggested a mousetrap model for NR activation in which the position of H-12 is different in liganded and unliganded (apo) states. H-12 is separated from the core LBD (inactive state) in the apo state, while H-12 moves to a more compact structure contacting the core LBD upon agonist binding (active state)[9]. Later studies revised

this mouse trap model of activation. They suggest that H-12 is dynamic and possibly non-helical in the apostate, and H-12 is only formed and stabilized upon agonist binding. This model suggests that more than a single active conformation of the FXR-LBD exists. Recent studies have shown differential effects of FXR agonists on FXR regulated gene expression, implying that FXR activation is more complex than the mechanism described by the mousetrap model[10]. These studies indicate that the unliganded FXR-LBD recruit corepressor such as nuclear receptor corepressor 1 (NCoR). Agonist binding stabilizes H-12 secondary structure and/or induces an H-12 conformational favorable to coactivator binding. Such agonist-induced changes lead to the recruitment of a coactivator (NCoA) and dissociation of the corepressor (**Fig. 8**).

In contrast, an inverse agonist stabilizes the interaction between the FXR-LBD and the corepressor by inducing an inactive state with a disordered H-12. Similar mechanisms have also been reported for other NRs like PPARγ[14]. Finally, there may be more than one AF-2 and H-12 structure that favors coactivator binding as different FXR ligands lead to different coactivator recruitment profiles[11,45].

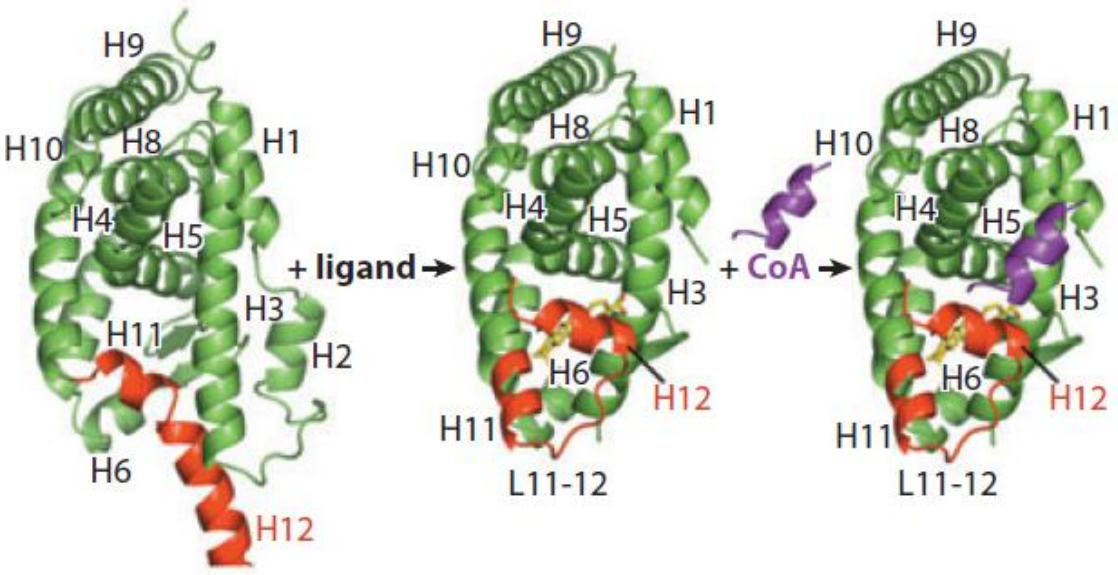

Fig. 8: Mousetrap model of FXR-LBD activation; binding of an agonist ligand stabilizes the H-12, allowing coactivator recruitment. (The model shown is of a different NR (RXR). [Figure adapted from *Huang et al., 2010*] [46]

2.6 FXR ligands

We have used commercially available FXR ligands, which have been previously characterized in cells and structure-function studies. These ligands include full and partial agonists that strongly or mildly enhance coactivator peptide recruitment, antagonists/non-agonists that keep coactivator peptide recruitment to a basal level. The chemical structure of FXR ligands used in this study is shown below (**Fig. 9**).

Tropifexor:

Tropifexor is a novel and highly potent nonsteroidal, non-bile acid FXR agonist under phase 2 human clinical trial to treat primary biliary cholangitis (PBC) and nonalcoholic steatohepatitis (NASH)[4,5].

XL335:

In vitro and *in vivo* optimization results indicate that XL335 is a potent and selective FXR agonist; oral administration to mice results in reduced cholesterol and triglycerides[47]. It is currently in phase 1 clinical trial.

GW4064:

GW4064 is a highly effective and selective nonsteroidal agonist of FXR, repressing the significant drug-metabolizing enzyme CYP3A4 expression in human hepatocytes[48]. GW4064 was found to raise HDL cholesterol levels and decrease triglycerides in various animal species[49]. Due to some limitations (solubility, toxicity, and UV stability), it is not considered a promising drug candidate. However, it is instead used as a tool compound to investigate the physiological functions of FXR[50]. Many nonsteroidal compounds have been made based on the GW4064 structure.

CDCA:

Chenodeoxycholic Acid (CDCA) is the essential steroidal endogenous bile acid ligand of FXR. CDCA bound FXR regulates the bile salt export pump expression, which is crucial in protecting liver damage[51]. Therefore, CDCA is more potent compared to other bile acids.

Fexaramine:

Fexaramine is a synthetic FXR agonist that has a higher affinity to FXR than endogenous ligands[61].

Ivermectin:

Ivermectin is a drug approved for nematode and arthropod parasites is a highly selective FXR antagonist. Treatment of wild-type mice with ivermectin resulted in lowering serum glucose and cholesterol levels. In addition, Ivermectin has shown antidiabetic activity by enhancing insulin sensitivity in an FXR-dependent manner[13]. Ivermectin is safe and well-tolerated in humans and forms the basis for the design of FXR antagonists for the treatment of metabolic diseases.

DY268:

DY268 has been identified to exhibit antagonistic activity towards FXR[52].

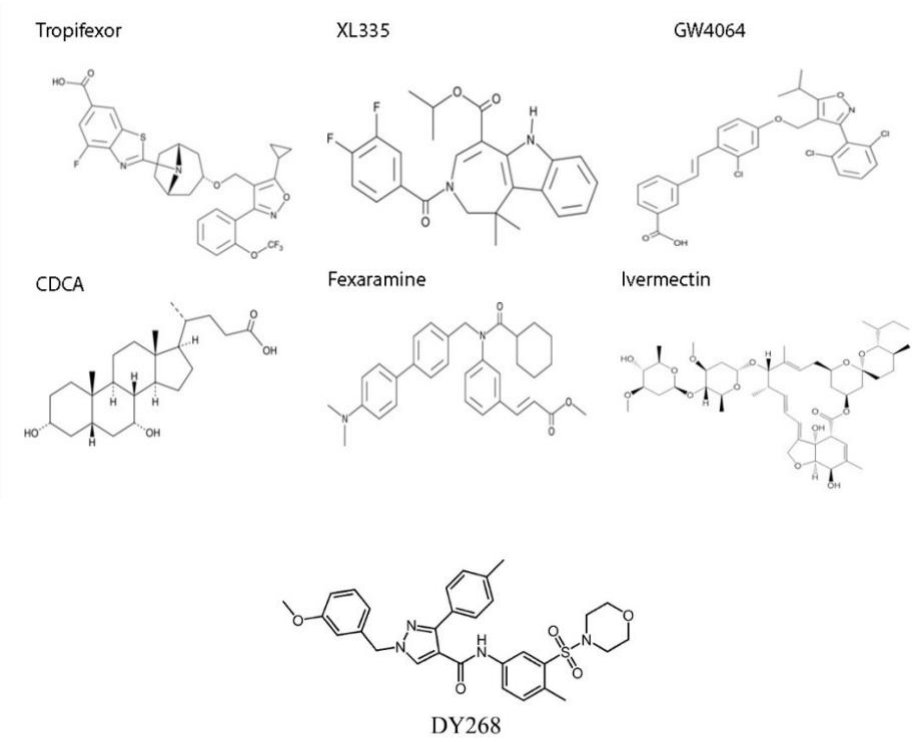

Fig. 9: Chemical structure of FXR ligands used in thesis research. [Figure adapted for DY268 is from *Jiang et al., 2021*][29]

2.7 Coactivator peptides: Steroid receptor coactivator (SRC)

Coactivators are a diverse group of proteins responsible for inducing conformational changes in agonist-bound NRs that are essential for NR-mediated transcriptional activation. A difference between coactivators and transcription factors is that coactivators do not directly bind DNA. Steroid receptor coactivators (SRCs) are one of the most studied families of coactivators and are implicated in a wide range of human diseases[53]. Unlike NRs, coactivator proteins appear mostly disordered; however, a short helical motif, termed the LXXLL motif[53], was identified within several coactivators (including SRCs),[54,55,] which binds to a hydrophobic pocket on the LBD. Several NRs have been co-crystalized with their cognate ligand and coactivator regions, including peptides, that contain the LXXLL motif within the NR interaction domain of coactivators. These structures reveal LXXLL motif binding is stabilized by interactions between the motif and the NR AF-2 surface region, including bonding between NR residues on H-3 and H-12 and the coactivator helix backbone amine and carbonyl groups. The SRCs contain three α-helical LXXLL motifs essential for their interaction with NRs. The sequences flanking these motifs are essential for NR selectivity[56.57]. SRCs are the most common coactivator for FXR, and most of the cocrystals of FXR are with SRC. The SRC LXXLL motif-containing peptides used in this work are fluorescein-labeled, namely SRC1-2 and SRC2-2 (Thermo Fisher Scientific). Our data shows that they have the highest affinity for FXR compared to other SRC family LXXLL motifs. **Table 1** shows these sequences of these peptides with the LXXLL motif in bold.

Table 1: SRC peptides and their sequences.

SRC peptide	Sequence
SRC1-2	LTERHKI**LHRLL**QEGSPSD
SRC2-2	LKEKHKI**LHRLL**QDSSSPV

3 Results:

3.1 FXR purification:

Due to the low solubility and yield of FXR-LBD, we have fused it with polyhistidine-tagged *Escherichia coli (E.coli)* maltose-binding protein (His_6-MBP). MBP enhances the solubility and improves the yield of its fusion protein partner, while the histidine tag facilitates purification by immobilized metal affinity chromatography (IMAC) using a nickel column[58]. Cleaving the MBP tag after IMAC purification using tobacco etch virus (TEV) protease digestion significantly decreased the stability and yield of FXR-LBD. At the same time, cleavage of the MBP tag did not significantly affect FXR-LBD activity, leading us to use MBP tagged FXR-LBD for all the experiments (**Fig. 10**). IMAC purification was followed by Fast protein liquid chromatography (FPLC) size exclusion purification. Only those fractions of MBP-FXR were selected from FPLC size-exclusion, which had the least amount of impurity. Based on the gel analysis, the major impurity appears to be MBP not fused to FXR (**Fig. 11**).

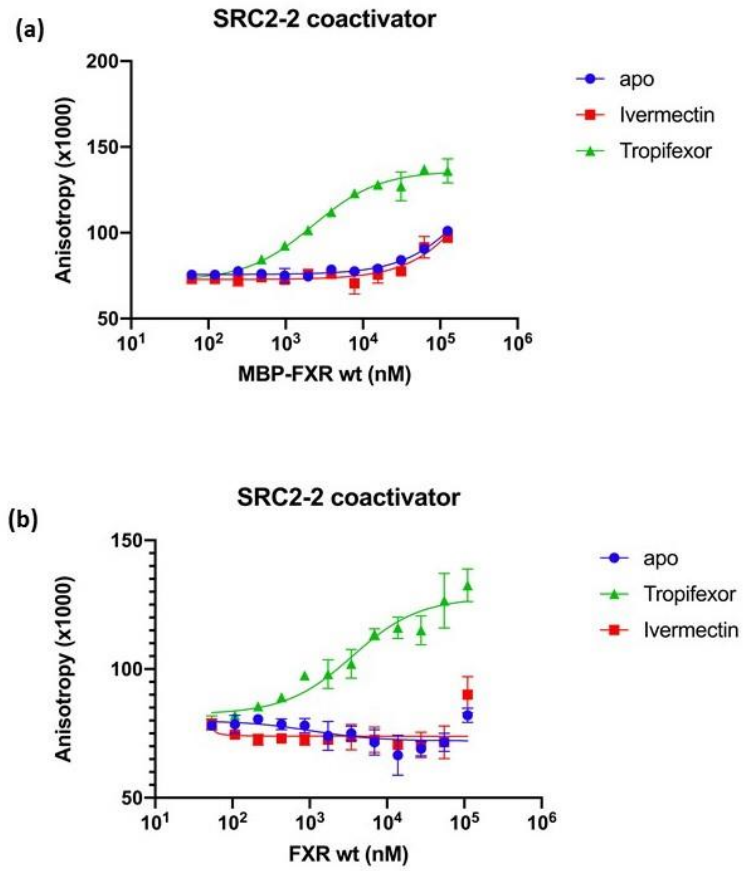

Fig. 10: Effect of MBP tag cleavage on FXR-LBD activity: Fluorescence anisotropy experiments measure the affinity of the coregulator peptide for FXR LBD in the absence (apo) and presence of an equimolar concentration of ligands. SRC2-2 efficacy for (**a**) MBP-FXR LBD wt (K_d (2.3 μM)) (**b**) MBP cleaved FXR-LBD wt (K_d (3.5 μM)). The data shown represent two technical replicates from a single experiment. **

**Refer to methods for sample preparation.

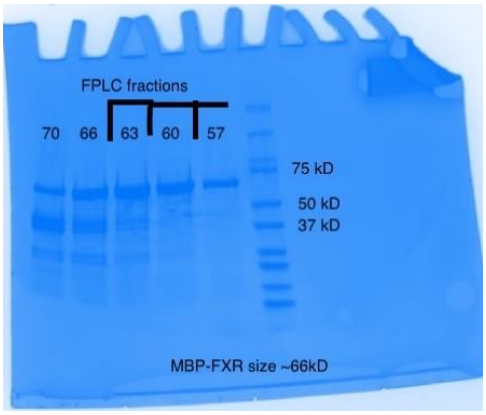

Fig. 11: SDS page gel of size exclusion purified MBP-FXR. Fractions up to 63 were collected for experiments.

3.2 The efficacy of different FXR ligands in coregulator peptide recruitment

We investigated the correlation of FXR coregulator binding surface structure with function (coactivator LXXLL motif peptide affinity) using FXR ligands of different efficacies in steroid receptor coactivator (SRC1-2 and SRC2-2) recruitment *in vitro*. In this study, we used six commercially available FXR ligands, including tropifexor,[1] XL335[47], and GW4064[48], which were reported to be agonists, CDCA an endogenous agonist[51], and ivermectin[13], which is reported to be an antagonist. We used fluorescence anisotropy (FA) to measure dissociation constants between fluoresceine-labeled coactivator peptides and FXR. The effect of the ligands mentioned above on FXR affinity for the coactivator peptide (SRC 2-2) is shown in (**Fig. 12a**). An increase in FA indicates increased binding of the coactivator peptide. A left shift of the curve indicates that a ligand increases the affinity of FXR for the peptide.

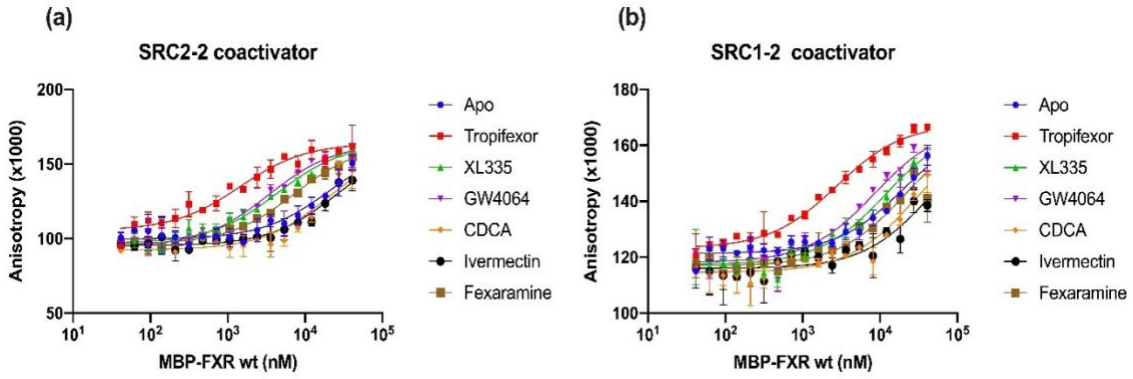

Fig. 12: Efficacy of FXR ligands: Fluorescence anisotropy experiments measure the affinity of the coregulator peptide for FXR LBD in the absence (apo) and presence of an equimolar concentration (41μM) of ligands. FXR ligands efficacy for (a) SRC2-2 or (b) SRC1-2 recruitment. The data shown represent two technical replicates from a single experiment.

The K_d values for coregulators interacting with FXR shown in **Table 2** indicate that Tropifexor is the most efficacious agonist. At the same time, Xl335 and GW4064 are less efficacious (partial agonists), and ivermectin has little effect, acting as an antagonist in this assay. A similar experiment using the same set of ligands and a different coactivator peptide (SRC 1-2) yielded similar results (**Fig. 12b**). Previous reports had characterized tropifexor, XL335, and GW4064 as agonists. However, our data show that they have variable efficacy.

Ivermectin has been reported to enhance the binding of both corepressor and coactivator peptides[13]. However, we found that ivermectin either decreases or has no effect on the affinity of FXR for SRC2-2 and SRC1-2 peptides. To examine the effects of ivermectin on corepressor peptide affinity, we performed FA of fluoresceine-labeled corepressor peptide SMRT ID2 (silencing mediator of retinoid and thyroid receptor, interaction domain 2) to

measure dissociation constants between SMRT ID2 and FXR using a known FXR antagonist ligand DY 268 as standard (**Fig. 13**). The K_d value of FXR-DY268 (9 μM) and FXR-ivermectin (42 μM) for SMRT ID2 combined with the fact that apo FXR shows no binding to SMRT ID2 indicate both ligands increase Ivermectin recruitment of SMRT. Along with our data showing reduced or no effect on coactivator binding, these data suggest that Ivermectin and DY268 are FXR antagonists and would likely function as inverse agonists on FXR target genes *in vivo*.

Table 2: Coactivator peptide affinity for FXR in the presence of ligands.

Ligands	SRC2-2	SRC1-2
	K_d (μM)	K_d (μM)
Apo	20.5	20
Tropifexor	1.4	2.7
XL335	4.3	11.8
GW4064	3.4	8.5
CDCA	20.7	29.3
Fexaramine	7.3	20.7
Ivermectin	26	44.5

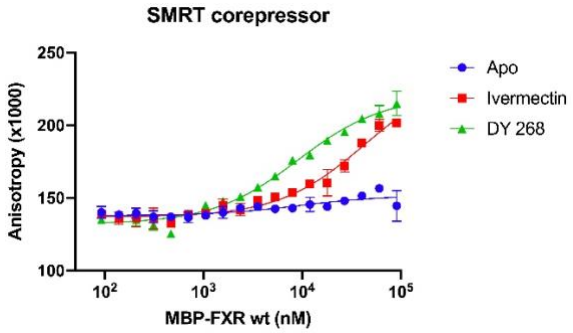

Fig. 13: Efficacy of antagonists (Ivermectin and DY268) of FXR in corepressor peptide (SMRT ID2) recruitment. The data shown represent the standard deviation from two technical replicates performed in a single experiment. NOTE: Elizabeth Sather purified the protein used in this anisotropy experiment.

3.3 H-12 conformational change observed by 19-F NMR

19-F NMR is a sensitive tool to observe structural changes[59]. We used 19F-NMR to observe the effect of ligands on H-12 dynamics. For these 19F NMR studies, a cysteine in MBP-FXR is covalently labeled (linked) with 3-Bromo-1,1,1-trifluoroacetate (BTFA), containing a trifluoromethyl (-CF3) group, the source of the fluorine signal. As the CF3 group rotates rapidly, this group produces a single NMR peak. Since MBP does not have any native cysteines while FXR LBD has three, BTFA labeling affects only the FXR LBD.

Wild-type FXR LBD contains three native cysteines on H-9 (C419), H-10 (C432), and H-12 (C466). The side chains of C432 and C466 appear to be solvent-exposed in a crystal structure of the FXR LBD (PDB ID: 3DCT); hence, they are most likely to be labeled with BTFA; in contrast, C419 is inside a hydrophobic pocket and is, therefore, less likely to get labeled (**Fig. 14**). We first determined which peaks arise from each of the three labeled cysteines by making receptors with a single mutation (C432H or C466S) and a double

mutant (DM) incorporating both these mutations. We replaced these cysteines with histidine and serine, respectively, because they are identical to the corresponding residues in murine FXRβ. A deconvoluted spectrum of FXR-LBD wt (2x BTFA post-label) bound to ivermectin shows a broad and a sharp peak (**Fig. 15a**) while C432H and C466S shows one broad and sharp peak, respectively indicating the source of each peak (**Fig. 15b,c**). Spectra of the double mutant show a well-separated, very weak, and ligand-responsive signal from the third cysteine (C419), indicating minimal exposure and labeling of this cysteine (**Fig. 16b**). In addition, the DM spectra show a larger signal that does not change upon ligand binding, which likely originates from labeled co-purifying proteins. We analyzed difference spectra where DM spectra are subtracted from C432H or C466S spectra to eliminate these unchanging signals.

C432H-DM difference spectra mutants (with DM spectra scaled down to 0.58 to avoid negative peaks) shows broad peaks for apo and ivermectin. Peak broadening indicates that H-12 is dynamic,[60] switching between multiple conformations on the microsecond to millisecond timescale in the absence of ligand (apo) and when bound to an antagonist (**Fig. 16a**). The binding of Tropifexor, the most efficacious agonist, results in a narrower, more consolidated spectrum. These NMR results indicate that H-12 dynamics correlate with an affinity for coactivators. Antagonist ligands and apo generate broad H-12 peaks, while efficacious agonists induce narrow H-12 NMR peaks consistent with a stable and structured H-12.

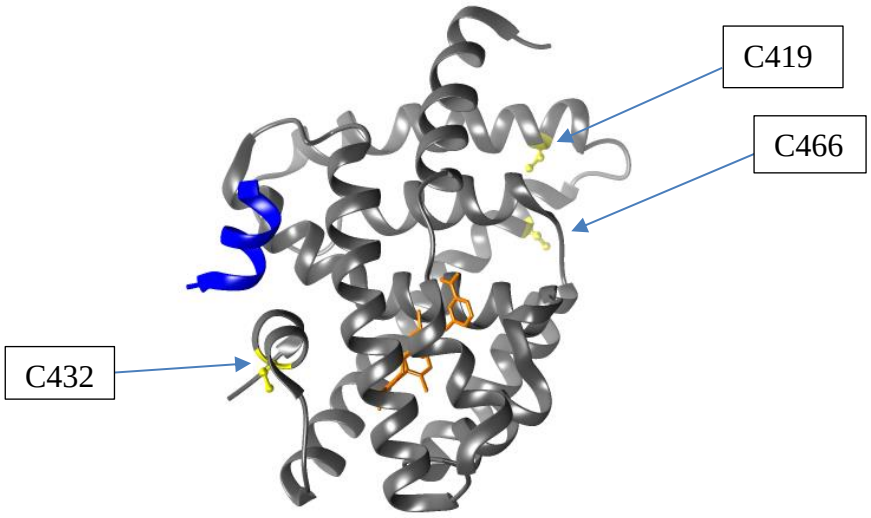

Fig. 14: The location of cysteines on the FXR-LBD [Figure adapted from*; PDB ID: 3DCT, modified*]

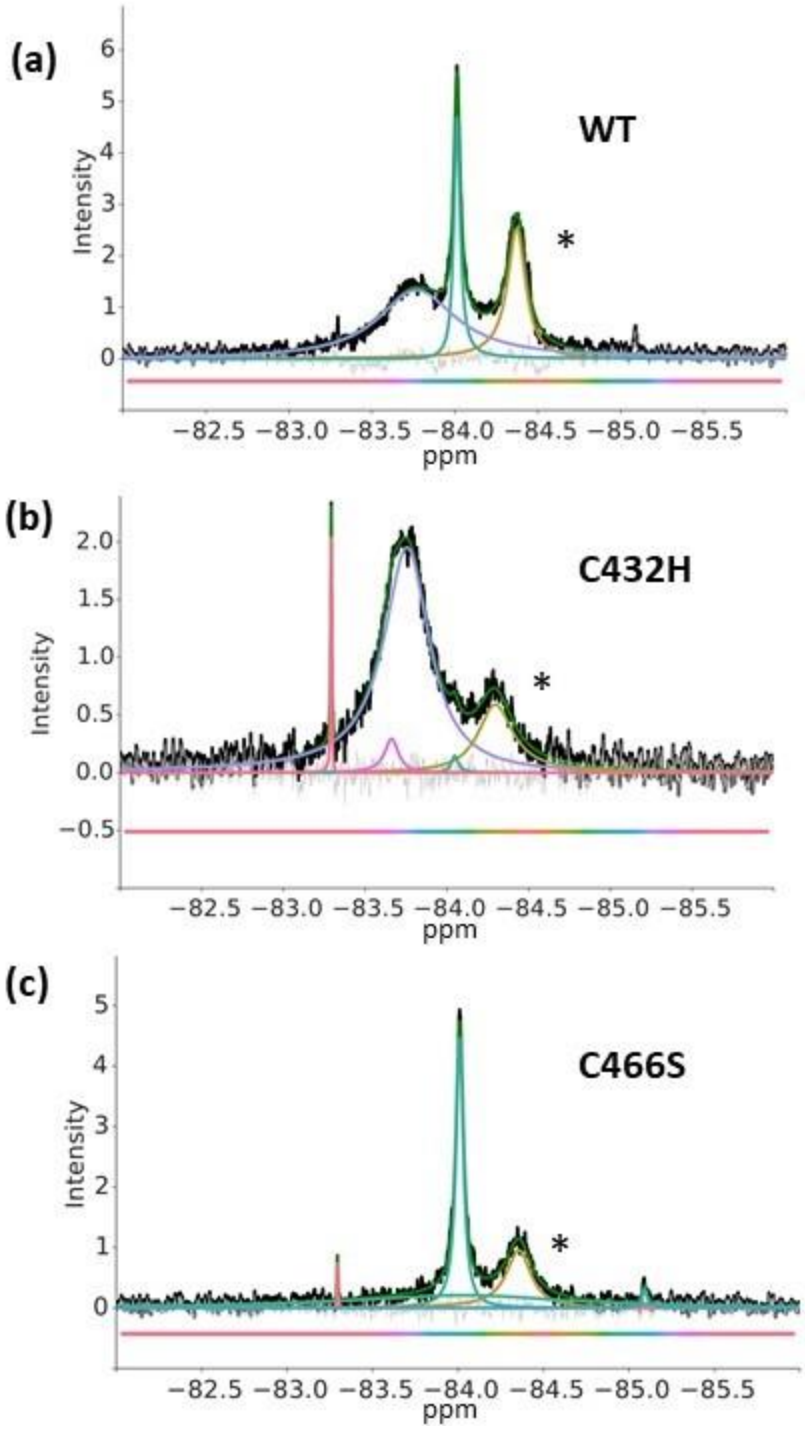

Fig. 15: Mutations in FXR-LBD bound to ivermectin to verify the source of peaks in 19F-NMR. Deconvoluted spectra of (a) FXR-LBD wt (b) C432H (c) C466S. peak on the rightmost side (*) is from impurity as the percentage of these peaks does not change, hence irrelevant here. **

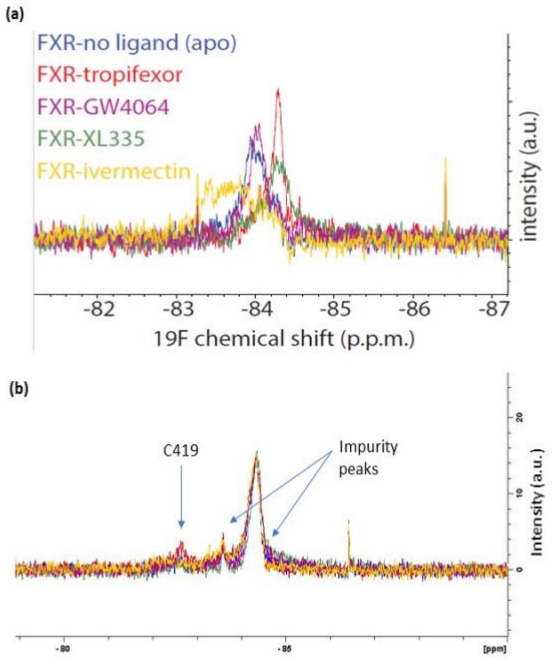

Fig. 16: 19-F NMR result of C432H and Double Mutant (C432H, C466S) MBP-FXR LBD-BTFA (pre-labeled) bound to different ligands and apoprotein. (a) C432H-DM difference spectrum (b) DM spectra.

We deconvoluted the difference spectra using our previously published method[60] to aid in spectral interpretation. The multiple peaks in the deconvoluted spectra indicate multiple FXR conformations, and the signal area of each peak indicates the relative population of each particular FXR conformation. For example, the deconvolution of C432H-DM difference spectra indicates a broad peak for apo and ivermectin bound FXR and sharper peaks for the partial and full agonists (**Fig. 17**). A list of major peaks in each spectrum and the contribution of each peak to the spectrum (%) is given in **Table 3**.

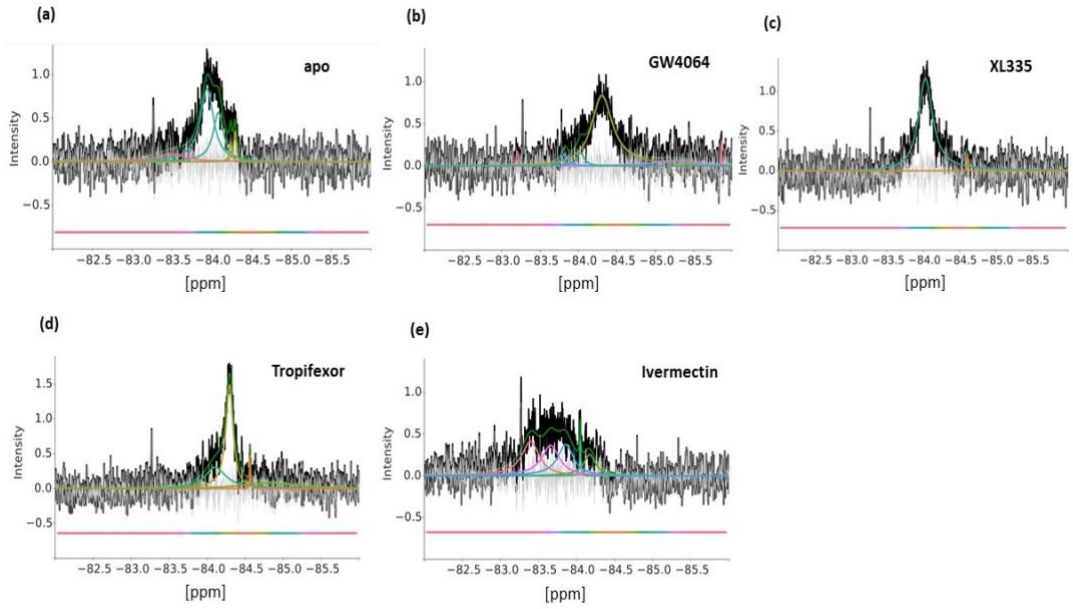

Fig. 17: Deconvoluted C432H-DM delta spectra. (a) apo (b) GW4064 (c) XL335 (d) Tropifexor (e) Ivermectin.

Table 3: List of the significant peak, size, and percentage of each spectrum in Fig. 16

Spectra	Peak (ppm) [**Hz**] [%]	Peak (ppm) [**Hz**] [%]	Peak (ppm) [**Hz**] [%]	Peak (ppm) [**Hz**] [%]	Peak (ppm) [**Hz**] [%]	Peak (ppm) [**Hz**] [%]
apo				(-84.086) [**105.051**] [27.8]		(-84.944) [**134.274**] [52.7]
GW4064					(-84.299) [**216.753**] [77.2]	
XL335				(-84.025) [**115.396**] [98.9]		
Tropifexor				(-84.100) [**217.206**] [29.2]	(-84.297) [**75.606**] [49.5]	
Ivermectin	(-83.399) [**183.610**] [31.4]	(-83.664) [**184.722**] [27.8]	(-83.861) [**164.761**] [25.5]	(-84.175) [**126.255**] [13.3]		

FA data shows that DY268 increases FXR affinity for a corepressor peptide (SMRT ID2) more than ivermectin. The FXR ivermectin complex with or without co-bound SMRT ID2 shows broad shifted peaks indicating considerable H-12 dynamics even after SMRT is recruited to this complex (**Fig. 18).** In contrast, DY268, the most efficacious in SMRT recruitment, induces an FXR 19F NMR spectrum with a much narrower peak (42 Hz), suggesting H-12 is relatively stable when bound to DY268. The addition of SMRT ID2 leads to a slightly broader and right-shifted peak (54 Hz), indicating slightly increased H-12 dynamics when SMRT is recruited (**Fig. 18**).

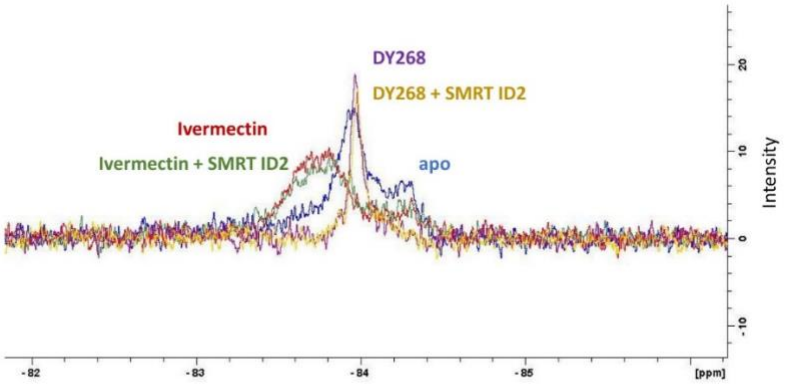

Fig. 18: C432H-DM difference spectrum of MBP-FXR-LBD-BTFA (pre-labeled) apo protein and bound to Ivermectin, DY268 and added SMRT ID2 corepressor. DM spectra were scaled down to 0.701 to avoid negative peaks. NOTE: Elizabeth Sather purified the protein and prepared and sent samples for NMR analysis for the spectra displayed in this figure.

Because H-12 contacts coactivators in published crystal structures, the addition of SRC1-2 coactivator peptide is expected to affect H-12 19F-spectra, as expected, the addition of SRC1-2 consolidates the two H-12 signals in FXR-agonist complexes (**Fig. 19**). This result is consistent with our previous work in PPARγ, where the addition of coactivators to agonist-receptor complexes led to H-12 19F-NMR signal consolidation[14].

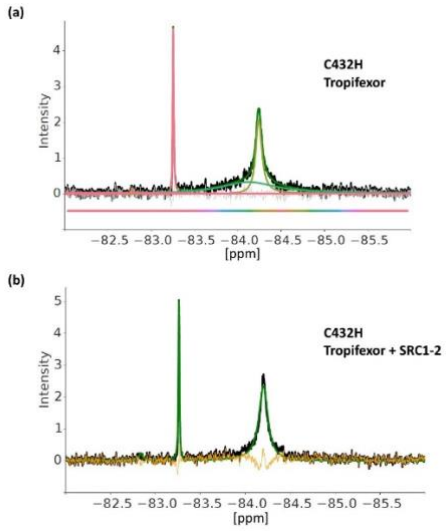

Fig. 19: Addition of a peptide, SRC1-2 changes the H-12 spectra and consolidates the two H-12 signals in FXR-agonist complexes. The deconvoluted spectrum of (a) FXR C432H bound to tropifexor (b) FXR C432H bound to tropifexor and peptide SRC1-2. **

Cleaving the MBP tag has no significant impact on the NMR signal from FXR LBD (**Fig. 20**), consistent with the anisotropy data that showed little impact of cleavage on FRX affinity for coactivators (**Fig. 10**). The process of cleaving the MBP increases purity (as determined by Coomassie stained gel, data not shown), therefore this impurity peak is missing in the cleaved FXR spectra.

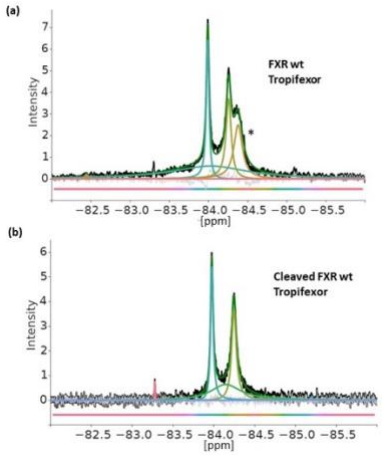

Fig. 20: Cleaving the MBP tag does not affect the 19F NMR signal. The deconvoluted spectrum of (a) FXR-MBP wt bound to tropifexor (b) FXR without MBP tag bound to tropifexor. The rightmost peak (*) in (a) is likely from impurity similar as explained in figure 15. **

3.4 Simulation confirms the 19F-NMR results

Helix 12 19F-NMR shows broad apo and ivermectin bound wild-type FXR signals, indicating a dynamic H-12. In contrast, FXR bound to the partial agonists XL335, GW4064, and especially the most efficacious agonist Tropifexor show narrower, more consolidated spectra indicative of less H-12 conformational heterogeneity. We ran conventional MD (cMD) simulations of apo and ligand-bound FXR to define better the structures and dynamics indicated by the 19F NMR spectra. Simulation models were built using the PDB crystal structure of FXR LBD bound to respective ligands in which H-12 is in the active conformation (**Table 3**).

Table 4: cMD builds and their corresponding PDB files.

cMD Build	PDB ID
Apo	3FLI
XL335	3FLI
Ivermectin	4WVD
GW4064	3DCT
Tropifexor	7D42
Tropifexor + SRC2-3	7D42

We ran six replicates of each simulation for a sufficiently long time to yield fairly consistent H-12 RMSD (average deviation over the sequence PLLCEI of H-12) relative to the starting structure (**Fig. 21**). The simulation for FXR bound to tropifexor and tropifexor with peptide SRC2-3 was in progress when this thesis was written and will be stopped and analyzed at ~100us, similar to other agonists complexes.

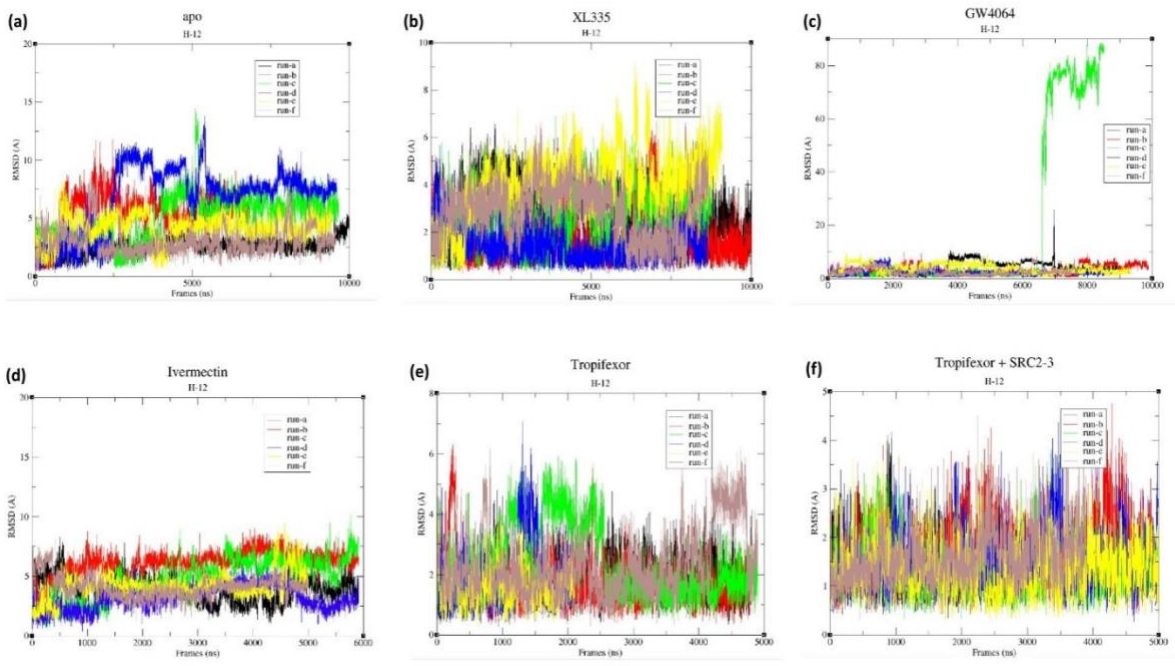

Fig. 21: MD simulations of wt FXR-LBD apo and bound to different ligands. Here we observe the convergence of H-12 RMSD relative to starting structure. The size of each frame is 10 ns.

Six independent simulations (approx. 100 μs each) of Apo FXR LBD indicate H-12 exchanges between many conformations distinct from the starting crystal structure (**Fig. 22a**). This result is consistent with the broad peak observed in 19F-NMR for apo FXR-LBD, indicating exchange between different H-12 conformations.

We built the ivermectin model from the only ivermectin-containing crystal structure available (4WVD). Because H-12 is not resolved in 4wvd, part of H-12 was added to 4wvd from another FXR crystal structure (3DCT) in Chimera. Six independent simulations (approx. 60 μs each) indicate that H-12 exchanges between distinct conformations when bound to ivermectin (**Fig. 22c**). These results are consistent with the 19F-NMR, which

shows a broad peak indicating conformational exchange of H-12 when bound to ivermectin.

Models for partial agonist XL335 and GW4064 bound FXR LBD were built using their crystal structures, 3FLI, and 3DCT, respectively. Six independent simulations (each XL335 simulation ran for approximately 100 μs while each GW4064 simulation ran for approximately 90 μs) indicate that partial agonist binding leads to primarily one major low energy conformation, H-12, which resembles the starting active H-12 conformation (**Fig. 22 b,d**). This result is consistent with the 19F-NMR result, where the XL335 and GW4064 produce single H-12, whereas apo FXR H-12 exchanges between two peaks.

The simulation model for full agonist Tropifexor was built using its crystal structure 7D42. 7D42 includes a bound coactivator (SRC2-3), which we removed for these simulations. Six independent simulations (each run for approx. 50 μs) indicate that H-12 occupies almost exclusively one major low energy conformation (**Fig. 22e**) similar to the starting active conformation in the crystal structure. This result is consistent with the 19F-NMR, where tropifexor induces the narrowest, most consolidated H-12 19F-NMR peak. These data indicate that the most efficacious agonist (tropifexor) is the most efficacious at stabilizing H-12. Likewise, the partial agonists provide both intermediate coactivator recruitment efficacy and stabilization of H-12.

We surmised that the addition of a coactivator would further stabilize H-12 in the FXR-tropifexor complex via interaction between H-12 and the coactivator. To verify this via

simulation, we built a simulation model of FXR bound to Tropifexor and a coactivator peptide SRC2-3 [KKKENAL**LRYLL**DKDDTKD] using crystal structure 7D42 (which includes the co-bound SRC2-3). We ran six independent simulations (approx. 40 μs each) and found that H-12 shows one sharp major low energy conformation (**Fig. 22f**), indicating that the binding of a coactivator may further stabilize H-12.

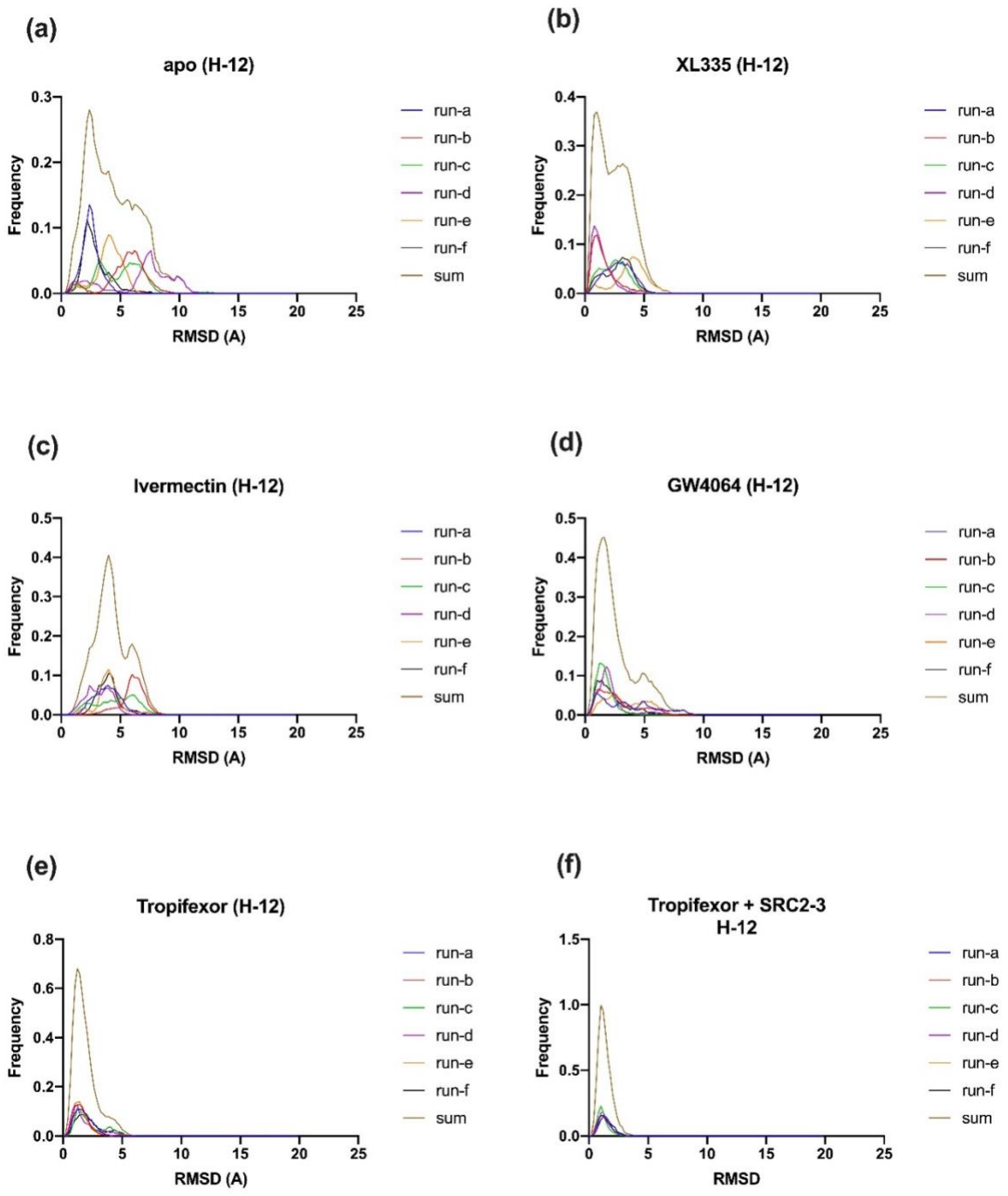

Fig. 22: Histogram of H-12 RMSD. The sum of RMSD frequencies for all the six independent runs for H-12 indicates the RMSD of most conformations. RMSD close to zero indicates conformations similar to starting crystal structure. FXR bound to (a) apo (b) Xl335 (c) Ivermectin (d) GW4064 (e) Tropifexor (f) Tropifexor and coactivator SRC2-3.

Observation of the RMSD fluctuation of ligands in the above simulations indicates that agonists stay primarily in one conformation. In contrast, antagonist conformation fluctuates in LBP shows some correlation between ligand fluctuation and H-12 stabilization (**Fig. 23**).

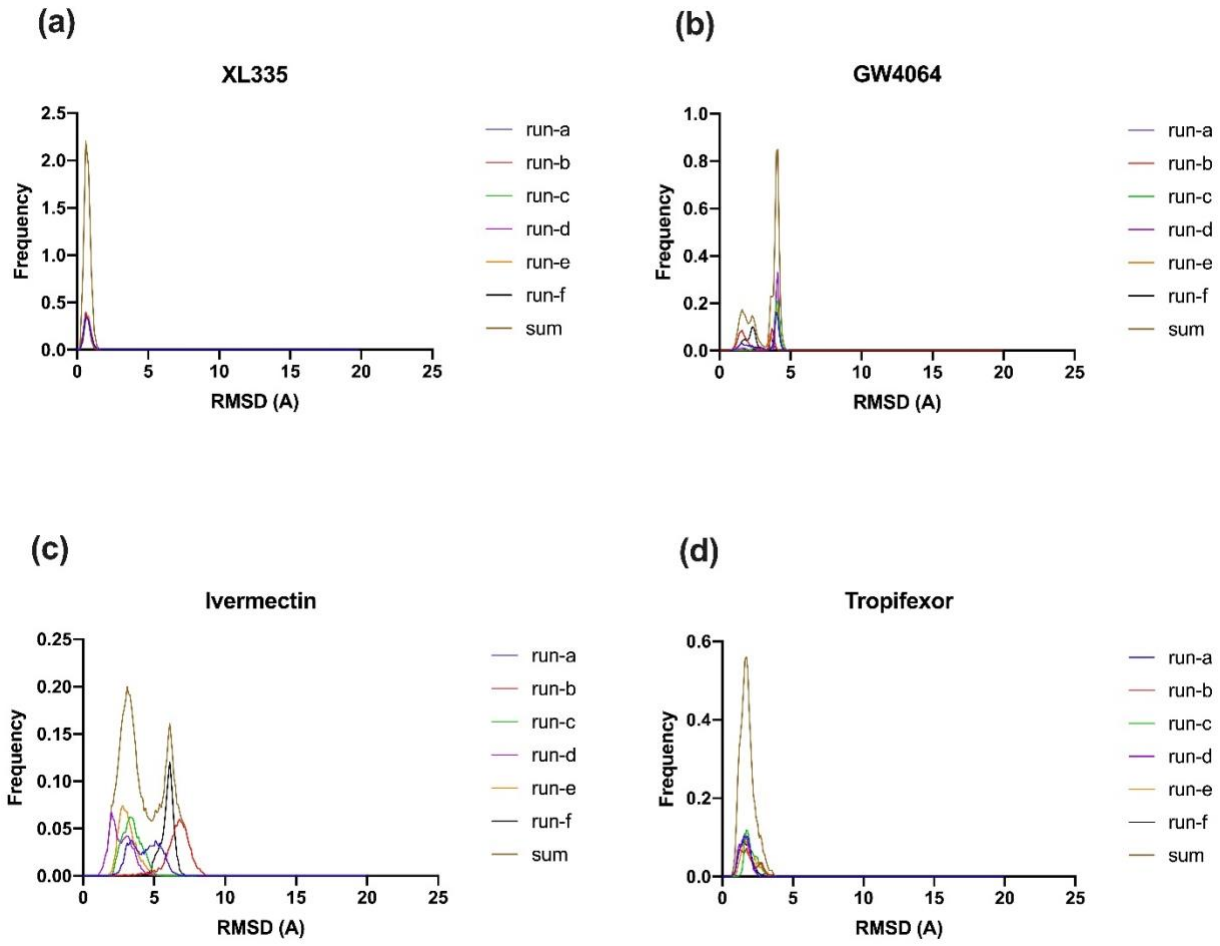

Fig. 23: RMSD fluctuations of ligand bound to LBP of FXR-LBD. (a) Ivermectin (b) XL335 (c) GW4064 (d) Tropifexor.

3.5 Discussion

FXR is a ligand-activated nuclear receptor that recruits coactivators upon binding agonists. The FXR conformational changes that result in increased affinity for coactivators are unclear. Our data suggest that conformational changes of H-12 are mainly responsible for FXR activity and coactivator recruitment; however, given that two partial agonists induce distinct H-12 structure and similar coactivator affinity, there are likely other structural aspects important to coactivator affinity.

Our data also suggest that the binding of ligands of different efficacies leads to different H-12 conformational ensembles. 19F-NMR and simulation data indicate that H-12 exchanges between multiple conformations on the microsecond to millisecond timescale for apo-FXR and in the presence of an antagonist (Ivermectin). In contrast, another antagonist/inverse agonist that induces the highest affinity for a corepressor peptide (DY268) induces mainly one H-12 conformation with a distinct chemical shift and likely distinct conformation from agonist bound FXR. There is currently no crystal structure available for FXR bound to DY268, so we could not perform a simulation of this complex. The binding of partial agonists, and to a larger degree, binding of a full agonist, stabilizes H-12 into a structurally active state which favors coactivator recruitment. 19F-NMR data clearly shows the most stabilization of H-12 (C432H mutant) by the most efficacious agonist (tropifexor) and inverse agonist (DY268) indicated by the sharp peaks. These data show a correlation between ligand efficacy and H-12 conformation.

Long-run simulation data are consistent with the 19F-NMR results. All simulations were started from FXR crystal structures with H-12 in the same active conformation. Simulation of Apo-FXR and Ivermectin-bound FXR results in various H-12 conformations different from the starting structure; such heterogeneity is expected to be conducive to forming a key hydrogen bond between the coactivator backbone and the H-12 charge clamp residue (E467)[31] or hydrophobic contact between H-12 and the coactivator. The simulation is consistent with 19F-NMR, where we see a broad peak of H-12 indicating μs to ms lifetime conformational exchange. Simulations of FXR bound to partial and strong agonists show that H-12 maintains a conformation similar to the starting PDB active structure [For the full agonist, Tropifexor, H-12 shows less variance from the starting structure than the partial agonists (XL335 and GW4064)]. The binding of agonists consolidates FXR LBD into a structurally active state that favors coactivator binding.

Interestingly the two partial agonists induce similar efficacy of coactivator recruitment but distinct H-12 conformational ensembles. This observation leaves open the possibility that these partial agonists could favor the recruitment of distinct sets of coactivators.

3.6 Conclusion

FXR plays a crucial role in protecting the liver and other organs via the regulation of bile acid and is crucial for regulating other metabolic processes, making FXR a potential therapeutic target for treating several liver-related disorders. The FXR-LBD shows multiple low-energy conformational states of the AF-2 coregulator binding surface. Upon

efficacious ligand binding, some of these states are favored, indicating that activation of FXR is more complex than a simple mousetrap model consisting of two well-defined states. Fluorescence anisotropy, solution 19F-NMR, and molecular dynamics data indicate that H-12 conformational changes are mainly responsible for FXR activity and coregulator recruitment which clarifies the structural model of FXR activation. We also found structural evidence that efficacious inverse agonists stabilize a distinct H-12 structure from efficacious agonists. Furthermore, H-12 exchanges between multiple conformations in Apo FXR and FXR bound to less efficacious agonists. This further defines the structural basis for graded agonism in FXR.

3.7 Future Directions

The two partial agonists, Xl335 and GW4064, induce distinct H-12 conformations as shown by solution 19F-NMR and molecular dynamics simulation but have similar coactivator affinity as shown by fluorescence data. These data indicate that there are likely other structural aspects important to coactivator affinity.

Regions apart from the AF-2 region, including H-11 can indirectly impact H-12 stabilization. In addition, the H-3 RMSD determined from molecular dynamics simulation data indicates that the binding of an agonist restricts the conformation of H-3 compared to apo and antagonist bound FXR (**Fig. 24**).

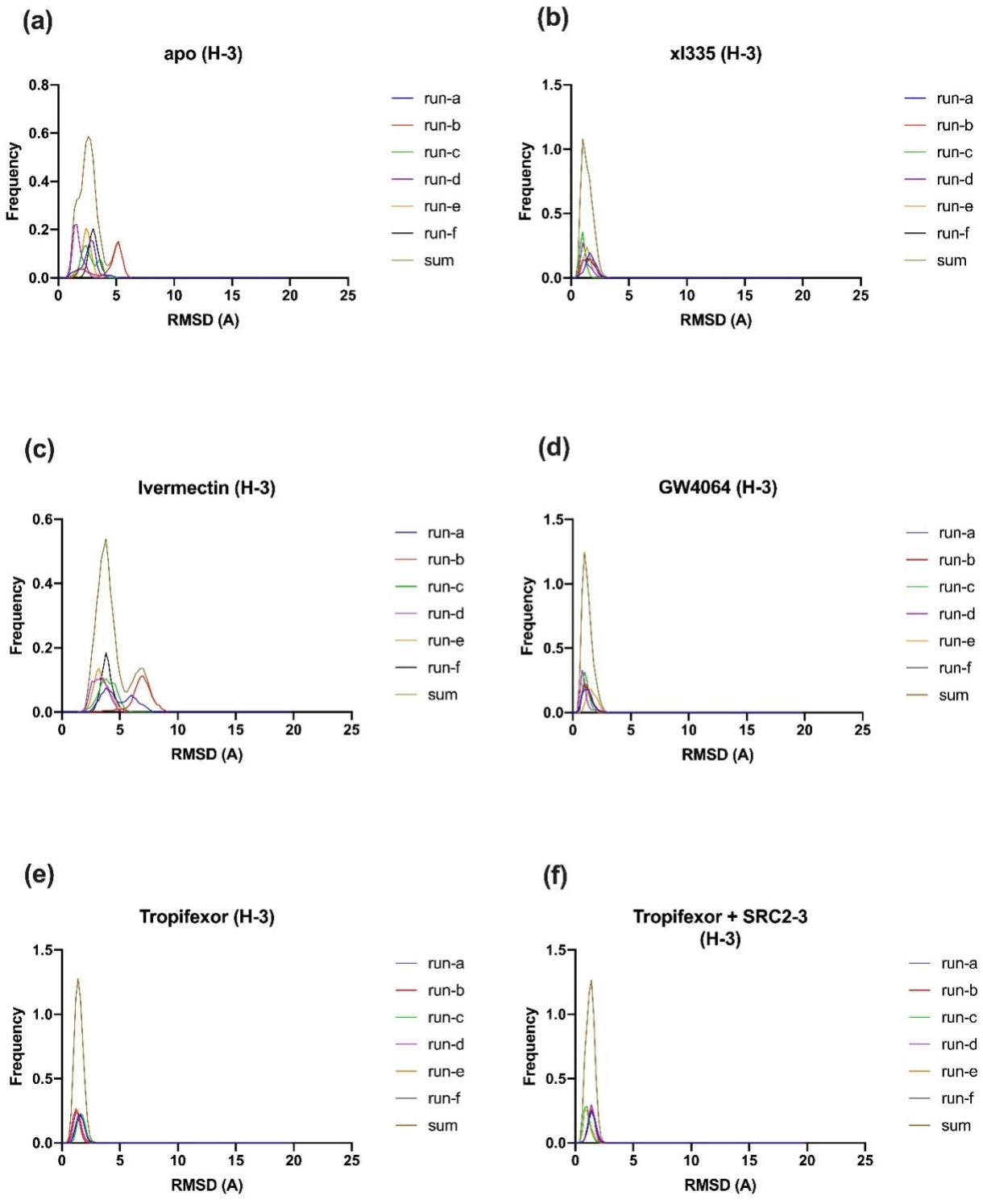

Fig. 24: H-3 RMSD of FXR when bound to different ligands. (a) apo (b) XL335 (c) Ivermectin (d) GW4064 (e) Tropifexor (f) Tropifexor + SRC2-3.

The simulation data can be verified using solution 19F-NMR by inserting a cysteine on H-3, as shown in **Figure 25**. To observe which region of H-3 shows the largest changes in conformation, we could make three individual cysteine mutations in the solvent-exposed residues (**Fig. 25**). This can give us insight into any correlation between H-3 stabilization and agonist binding.

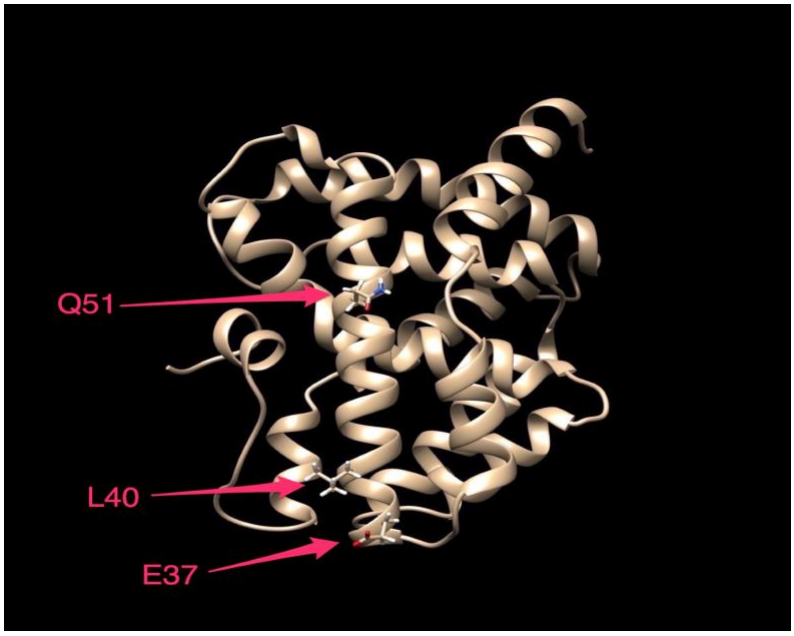

Fig. 25: Position of residues on H-3 for possible single cysteine mutations to observe H-3 dynamics via 19F-NMR. [Figure adapted from*; PDB ID: 3DCT, modified*]

4 Methods

The protocol of the methods used in this work is very much similar to one of our labs' previous published work[14].

4.1 Protein purification

A pDEST-566 plasmid [pDest-566 was a gift from Dominic Esposito (Addgene plasmid #11517; http://n2t.net/addgene:11517; RRID: Addgene_11517)] carrying the gene for ampicillin resistance and N-terminally 6xHis-MBP tagged FXR containing a tobacco etch virus (TEV) nuclear inclusion protease recognition site between the MBP tag and protein [6xHis-MBP-TEV-FXR] of interest was transformed into chemically competent *E.coli* BL21 (DE3) Gold cells. Cells were grown in either terrific broth (TB) or Luria broth (LB). Cells grown in TB media at 37 °C were induced at an OD_{600} of 0.6-0.8 by adding 0.5 mM isopropyl β-D-1-thiogalactopyranoside (IPTG), and the temperature was lowered to 18 °C. Induction proceeded for 16-18 h before harvesting. Harvested cells were homogenized into 20 mM Tris-base (pH 7.5), 500 mM NaCl, 5 mM tris(2-carboxyethyl) phosphine (TCEP), 10% glycerol, 20 mM imidazole and lysed using a C-5 Emulsiflex high-pressure homogenizer (Avestin). Lysates were then clarified (centrifugation at 19,000 g for 45 minutes and filtered through a 0.45 μm filter) and passed through two Histrap FF 5 ml columns in series (GE Healthcare) overnight at a flow rate of 1 ml/min using an AKTA start (GE Healthcare). Protein was eluted using a gradient from 20 to 250 mM imidazole. Fast protein liquid chromatography was performed on AKTA start (GE Healthcare). The eluted 6xHis-MBP FXR was further purified by size exclusion chromatography (SEC) gel

filtration using HiLoad Superdex 75 (GE Healthcare). SEC was performed in 50 mM Tris-base (PH 8.3), 500 mM NaCl, 10 mM TCEP, 10% glycerol buffer. Protein purity was determined by sodium dodecyl sulfate-polyacrylamide gel electrophoresis (SDS-PAGE) analysis (Bio-Rad).

4.2 FXR-LBD sequence used in this work: 246-472

T P D Q Q T L L H F I M D S Y N K Q R M P Q E I T N K I L K E E F S A E E N F L I
L T E M A T N H V Q V L V E F T K K L P G F Q T L D H E D Q I A L L K G S A V
E A M F L R S A E I F N K K L P S G H S D L L E E R I R N S G I S D E Y I T P M F
S F Y K S I G E L K M T Q E E Y A L L T A I V I L S P D R Q Y I K D R E A V E K L
Q E P L L D V L Q K L C K I H Q P E N P Q H F A C L L G R L T E L R T F N H H H
A E M L M S W R V N D H K F T P L L C E I W D V Q

4.3 Site-directed mutagenesis

Mutations in FXR LBD were generated using the Quickchange II site-directed mutagenesis kit (Agilent) using primers listed in **Table 5**. The presence of the expected mutation and absence of spurious mutations was confirmed by Sanger sequencing (Eurofins).

Table 5: **Primer sequences used for mutagenesis**

C432H	5’ -caggcgacccaggagatgggcaaagtgttgagga-3’
C466S	5’ -cgtcccagatttcagagagaagtggggtaaactt-3’

4.4 Fluorescence anisotropy (FA) assay

FA peptide binding assay was performed by plating a mixture of 50 nM peptide with an N-terminal FITC tag, 12-point serial dilutions (1:2) of MBP-FXR LBD wt, and FXR ligands from approx. 50 μM to 24 nM. FXR-LBD and FXR ligands were added at a 1:1 ratio. This mixture was added to wells of low-volume 384-well black plates (Grenier Bio-one, catalog number 784076) to a final volume of 16 μl. Peptides were purchased from ThermoFisher (Waltham, MA, USA) for SRC1-2 peptide, sequence: LTERHKILHRLLQEGSPSD (19); SRC2-2 peptide, sequence: LKEKHKILHRLLQDSSSPV (19). All dilutions were made in SEC buffer (pH 8.3), 0.01% fatty-acid-free bovine albumin (BSA) (EMD Millipore, catalog number 126575), 0.01% Tween. Assay titrations were performed in duplicate. Plates were incubated in the dark at room temperature for 2 hours before being read by a Synergy H1 microplate reader (BioTek). FA was measured by excitation at 485 nm/20 nm and emission at 528 nm/20 nm for FITC/5-FAM. Data were fit using nonlinear regression (agonist vs. response-variable slope 4 parameters) in Prism 9.0.0.

Some of the previous samples for fluorescence anisotropy were prepared using 20 mM Tris-base, 150 mM NaCl, 25 mM imidazole, and 10% glycerol at pH 8.0. ** Samples were prepared by this method in Figure 10.

4.5 Preparation of 19F-NMR samples

19F-NMR samples were prepared to a final concentration of 41 μM protein in 520 ul volume containing 10% D_2O. The addition of ligand was done in two separate injections

of the compound to reduce precipitation. Injections were spaced 20-30 min apart to allow time for binding. All ligands were dissolved in D6-dimethylsulfoxide (DMSO). Deuterated solvents were obtained from Cambridge Isotope Laboratories Inc. and were at least 99% isotopically pure. The final concentrations of ligand for all samples were 1x ligand to the protein. FXR mutant proteins were purified by first lysing *E.coli* cells and then went through centrifugation at 19,000 g for 1 h, then labeled with 0.1% BTFA (9.63 M stock) added to the lysate, incubated at 4 °C for 15-20 minutes, then filtered using a 0.45 μm filter before IMAC His-tag purification. NMR samples were prepared by buffer exchanging protein samples >100x into 50 mM NaCl, 50 mM Tris-base, 10mM TCEP, 10% glycerol (pH 8.3) using 30 kD MWCO Amicon Ultra-15 concentrators (Merck Millipore) to remove excess NaCl. After the ligands were added in a 1:1 ratio in two steps at an interval of 15-20 min to avoid ligand precipitation, followed by the addition of buffered D_2O.

Some previous 19F-NMR samples were prepared using different buffer conditions and labeling. MBP-FXR LBD purified in 20 mM Tris base, 150 mM NaCl, 25 mM imidazole and 10% glycerol at pH 8.0. 2X BTFA was labeled after purification and incubated at 4C overnight. Samples were buffer exchanged in 25mM MOPS, 25mM KCl and 1mM EDTA >100x. The rest of the methods were the same as explained earlier. **Samples were prepared by this method in Figures 15, 19, and 20.

4.6 Molecular dynamics simulation

Missing residues in the crystal structure compared to our FXR LBD construct used in NMR were added using the modeler in Chimera software, and a PDB file was saved. This PDB file was then submitted to the h++ server (http://biophysics.cs.vt.edu/H++) to determine the state of titratable protons at pH 7.4 along with more realistic rotamers for some residues. This h++ PDB file was then given AMBER residue names using pdb4amber (AmberTools14). The ligand from this PDB file was removed, and hydrogens were added in Chimera then submitted to the RED server for RESP charge assignment. The output mol2 file was then used to prepare a gaff2 file and a force modification file (frcmod). Tleap was then used to generate parameter and coordinate files using ff14SB and GAFF2 values. A truncated octahedron solvation cell with boundaries at least 10 Å from any protein atom was built with TIP3P water. The system was neutralized with Na^+ ions, and K^+ and Cl^- ions were added to 0.5 M. Joung and Cheatham ion parameters were used. Minimization (imin = 1) and equilibration were carried out in nine steps with non-bonded cutoff set to 8 Å and with the equilibrations carried out at 310 K. The final restart file from this process was used along with a hydrogen mass repartitioned parameter file (modified using parmed) to run new simulations with new randomized atomic velocities using 4 fs steps at 310 K. Analysis was carried out using CPPTRAJ. All production simulations were carried out using pmemd.cuda.

REFERENCES

1. Tully, D. C. et al. (2017). Discovery of Tropifexor (LJN452), a Highly Potent Non-bile Acid FXR Agonist for the Treatment of Cholestatic Liver Diseases and Nonalcoholic Steatohepatitis (NASH). *Journal of Medicinal Chemistry*, *60*(24), 9960–9973.
2. Zhang, Y. et al. (2003). Natural Structural Variants of the Nuclear Receptor Farnesoid X Receptor Affect Transcriptional Activation. *Journal of Biological Chemistry*, *278*(1), 104–110.
3. Kliewer, S. A., & Mangelsdorf, D. J. (2015). Bile Acids as Hormones: The FXR-FGF15/19 Pathway. *Digestive Diseases*, *33*(3), 327–331.
4. Fang, S. et al. (2015). Intestinal FXR agonism promotes adipose tissue browning and reduces obesity and insulin resistance. *Nature Medicine*, *21*(2), 159–165.
5. Pellicciari, R. et al. (2002). 6α-Ethyl-Chenodeoxycholic acid (6-ECDCA), a Potent and Selective FXR Agonist Endowed with Anticholestatic Activity. *Journal of Medicinal Chemistry*, *45*(17), 3569–3572.
6. Genin, M. J. et al. (2015). Discovery of 6-(4-{[5-Cyclopropyl-3-(2,6-dichlorophenyl)isoxazol-4-yl]methoxy}piperidin-1-yl)-1-methyl-1H-indole-3-carboxylic Acid: A Novel FXR Agonist for the Treatment of Dyslipidemia. *Journal of Medicinal Chemistry*, *58*(24), 9768–9772.
7. Lamers, C., Schubert-Zsilavecz, M., & Merk, D. (2014). Medicinal Chemistry and Pharmacological Effects of Farnesoid X Receptor (FXR) Antagonists. *Current Topics in Medicinal Chemistry*, *14*(19), 2188–2205.
8. Aranda, A., & Pascual, A. (2001). Nuclear Hormone Receptors and Gene Expression. *Physiological Reviews*, *81*(3), 1269–1304.

9. Renaud, J. P. et al. (1995). Crystal structure of the RAR-γ ligand-binding domain bound to all-trans retinoic acid. *Nature*, *378*(6558), 681–689.
10. Rastinejad, F., Ollendorff, V., & Polikarpov, I. (2015). Nuclear receptor full-length architectures: confronting myth and illusion with high resolution. *Trends in Biochemical Sciences*, *40*(1), 16–24.
11. Downes, M. et al. (2003). A Chemical, Genetic, and Structural Analysis of the Nuclear Bile Acid Receptor FXR. *Molecular Cell*, *11*(4), 1079–1092.
12. Zheng, W. et al. (2017). recently approved Novel Class of Natural FXR Modulators with a Unique Mode of Selective Co-regulator Assembly. *ChemBioChem*, *18*(8), 721–725.
13. Jin, L. et al. (2013). The antiparasitic drug ivermectin is a novel FXR ligand that regulates metabolism. *Nature Communications*, *4*(1).
14. Chrisman, I. M. et al. (2018). Defining a conformational ensemble that directs activation of PPARγ. *Nature Communications*, *9*(1).
15. Bain, D. L. et al. (2007). Nuclear Receptor Structure: Implications for Function. *Annual Review of Physiology*, *69*(1), 201–220.
16. Kramer, I. M. (2021). *Signal Transduction, Third Edition by Ijsbrand M. Kramer (2015–12-05)*. Academic Press; 3rd edition (2015–12-05).
17. Weikum, E. R., Liu, X., & Ortlund, E. A. (2018b). The nuclear receptor superfamily: A structural perspective. *Protein Science*, *27*(11), 1876–1892.
18. Xu, E. H., & Lambert, M. H. (2003). Structural insights into the regulation of nuclear receptors by ligands. *Nuclear Receptor Signaling*, *1*(1), nrs.01004.
19. Gronemeyer, H., & Moras, D. (1995). How to finger DNA. *Nature*, *375*(6528), 190–191.
20. Xu, J., & Li, Q. (2003). Review of the in Vivo Functions of the p160 Steroid Receptor Coactivator Family. *Molecular Endocrinology*, *17*(9), 1681–1692.
21. Pascual, A. P. (2001). Aranda A, (2001) Nuclear hormone receptors and gene expression. *Physiol Rev 81*, 1260–1304.

22. Meier, C. A. (1997). Minireview: Regulation of Gene Expression by Nuclear Hormone Receptors. *Journal of Receptors and Signal Transduction*, *17*(1–3), 319–335.

23. Tenbaum, S. T. (1997). Nuclear receptors: structure, function, and involvement in disease. (1997). Int J Biochem Cell Biol, 29, 1325–1341. *Int J Biochem Cell Biol*, *29*, 1325–1341.

24. Resche-Rigon, M., & Gronemeyer, H. (1998). Therapeutic potential of selective modulators of nuclear receptor action. *Current Opinion in Chemical Biology*, *2*(4), 501–507.

25. Makishima, M. (1999). Identification of a Nuclear Receptor for Bile Acids. *Science*, *284*(5418), 1362–1365.

26. Cai, S. Y. et al. (2007). The farnesoid X receptor FXRα/NR1H4 acquired ligand specificity for bile salts late in vertebrate evolution. *American Journal of Physiology-Regulatory, Integrative and Comparative Physiology*, *293*(3), R1400–R1409.

27. Otte, K. et al. (2003). Identification of Farnesoid X Receptor β as a Novel Mammalian Nuclear Receptor Sensing Lanosterol. *Molecular and Cellular Biology*, *23*(3), 864–872.

28. Renga, B. et al. (2009). Reciprocal regulation of the bile acid-activated receptor FXR and the interferon-γ-STAT-1 pathway in macrophages. *Biochimica et Biophysica Acta (BBA) - Molecular Basis of Disease*, *1792*(6), 564–573.

29. Jiang, L. et al. (2021). Farnesoid X receptor (FXR): Structures and ligands. *Computational and Structural Biotechnology Journal*, *19*, 2148–2159.

30. Han, C. (2018). Update on FXR Biology: Promising Therapeutic Target? *International Journal of Molecular Sciences*, *19*(7), 2069.

31. Merk, D. et al. (2019). Molecular tuning of farnesoid X receptor partial agonism. *Nature Communications*, *10*(1).

32. Neuschwander-Tetri, B. A. et al. (2015). Farnesoid X nuclear receptor ligand obeticholic acid for non-cirrhotic, nonalcoholic steatohepatitis (FLINT): a multicentre, randomized, placebo-controlled trial. *The Lancet*, *385*(9972), 956–965.

33. Hirschfield, G. M. et al. (2015). Efficacy of Obeticholic Acid in Patients With Primary Biliary Cirrhosis and Inadequate Response to Ursodeoxycholic Acid. *Gastroenterology*, *148*(4), 751–761.e8.

34. Mudaliar, S. et al. (2013). Efficacy and Safety of the Farnesoid X Receptor Agonist Obeticholic Acid in Patients With Type 2 Diabetes and Nonalcoholic Fatty Liver Disease. *Gastroenterology*, *145*(3), 574–582.e1.

35. Devarakonda, S. (2003). Structure of the heterodimeric ecdysone receptor DNA-binding complex. *The EMBO Journal*, *22*(21), 5827–5840.

36. Zhang, Y., Kast-Woelbern, H. R., & Edwards, P. A. (2003b). Natural Structural Variants of the Nuclear Receptor Farnesoid X Receptor Affect Transcriptional Activation. *Journal of Biological Chemistry*, *278*(1), 104–110.

37. Laffitte, B. A. et al. (2000). Identification of the DNA Binding Specificity and Potential Target Genes for the Farnesoid X-activated Receptor. *Journal of Biological Chemistry*, *275*(14), 10638–10647.

38. Claudel, T. et al. (2002). Bile acid-activated nuclear receptor FXR suppresses apolipoprotein A-I transcription via a negative FXR response element. *Journal of Clinical Investigation*, *109*(7), 961–971.

39. Zhan, L. et al. (2014). Genome-Wide Binding and Transcriptome Analysis of Human Farnesoid X Receptor in Primary Human Hepatocytes. *PLoS ONE*, *9*(9), e105930.

40. Wang, N. et al. (2018). Ligand binding and heterodimerization with retinoid X receptor α (RXRα) induce farnesoid X receptor (FXR) conformational changes affecting coactivator binding. *Journal of Biological Chemistry*, *293*(47), 18180–18191.

41. Zheng, W. et al. (2018). Structural insights into the heterodimeric complex of the nuclear receptors FXR and RXR. *Journal of Biological Chemistry*, *293*(32), 12535–12541.

42. Wang, Y. D. et al. (2008). FXR: a metabolic regulator and cell protector. *Cell Research*, *18*(11), 1087–1095.

43. Mi, L. Z. et al. (2003). Structural Basis for Bile Acid Binding and Activation of the Nuclear Receptor FXR. *Molecular Cell*, *11*(4), 1093–1100.

44. Jiang, L. et al. (2021). Structural basis of tropifexor as a potent and selective agonist of farnesoid X receptor. *Biochemical and Biophysical Research Communications*, *534*, 1047–1052.

45. Soisson, S. M. et al. (2008). Identification of a potent synthetic FXR agonist with an unexpected mode of binding and activation. *Proceedings of the National Academy of Sciences*, *105*(14), 5337–5342.

46. Huang, P. et al. (2010). Structural Overview of the Nuclear Receptor Superfamily: Insights into Physiology and Therapeutics. *Annual Review of Physiology*, *72*(1), 247–272.

47. Flatt, B. et al. (2009). Discovery of XL335 (WAY-362450), a Highly Potent, Selective, and Orally Active Agonist of the Farnesoid X Receptor (FXR). *Journal of Medicinal Chemistry*, *52*(4), 904–907.

48. Zhang, S., Pan, X., & Jeong, H. (2015). GW4064, an Agonist of Farnesoid X Receptor, Represses CYP3A4 Expression in Human Hepatocytes by Inducing Small Heterodimer Partner Expression. *Drug Metabolism and Disposition*, *43*(5), 743–748.

49. Sinal, C. J. et al. (2000). Targeted Disruption of the Nuclear Receptor FXR/BAR Impairs Bile Acid and Lipid Homeostasis. *Cell*, *102*(6), 731–744.

50. Li, W. et al. (2012). Unbinding Pathways of GW4064 from Human Farnesoid X Receptor as Revealed by Molecular Dynamics Simulations. *Journal of Chemical Information and Modeling*, *52*(11), 3043–3052.

51. Hanafi, N. I. et al. (2018). Overview of Bile Acids Signaling and Perspective on the Signal of Ursodeoxycholic Acid, the Most Hydrophilic Bile Acid, in the Heart. *Biomolecules*, *8*(4), 159.

52. Yu, D. D., Lin, W., Forman, B. M., & Chen, T. (2014). Identification of trisubstituted-pyrazole carboxamide analogs as novel and potent antagonists of farnesoid X receptor. *Bioorganic & Medicinal Chemistry*, *22*(11), 2919–2938.

53. Johnson, A. B., & O'Malley, B. W. (2012). Steroid receptor coactivators 1, 2, and 3: Critical regulators of nuclear receptor activity and steroid receptor modulator (SRM)-based cancer therapy. *Molecular and Cellular Endocrinology*, *348*(2), 430–439.

54. Heery, D. M. et al. (1997). A signature motif in transcriptional coactivators mediates binding to nuclear receptors. *Nature*, *387*(6634), 733–736.

55. Torchia, J. et al. (1997). The transcriptional coactivator p/CIP binds CBP and mediates nuclear-receptor function. *Nature*, *387*(6634), 677–684.

56. Chang, C. Y. et al. (1999). Dissection of the LXXLL Nuclear Receptor-Coactivator Interaction Motif Using Combinatorial Peptide Libraries: Discovery of Peptide Antagonists of Estrogen Receptors α and β. *Molecular and Cellular Biology*, *19*(12), 8226–8239.

57. Coulthard, V. H., Matsuda, S., & Heery, D. M. (2003). An Extended LXXLL Motif Sequence Determines the Nuclear Receptor Binding Specificity of TRAP220. *Journal of Biological Chemistry*, *278*(13), 10942–10951.

58. Raran-Kurussi, S., & Waugh, D. S. (2017). Expression and Purification of Recombinant Proteins in Escherichia coli with a His_6 or Dual His_6-MBP Tag. *Methods in molecular biology (Clifton, N.J.)*, *1607*, 1–15.

59. Kitevski-LeBlanc, J. L., & Prosser, R. S. (2012b). Current applications of 19F NMR to studies of protein structure and dynamics. *Progress in Nuclear Magnetic Resonance Spectroscopy*, *62*, 1–33.

60. Hughes, T. S. et al., (2015). Deconvolution of Complex 1D NMR Spectra Using Objective Model Selection. *PLOS ONE*, *10*(8), e0134474.

61. Downes, M. et al., (2003). A Chemical, Genetic, and Structural Analysis of the Nuclear Bile Acid Receptor FXR. *Molecular Cell*, *11*(4), 1079–1092.